

NATIONAL ADVISORY COMMITTEE FOR AERONAUTICS

TECHNICAL NOTE 2141

CHARTS FOR ESTIMATING DOWNWASH BEHIND
RECTANGULAR, TRAPEZOIDAL, AND
TRIANGULAR WINGS AT SUPERSONIC
SPEEDS

By Rudolph C. Haefeli, Harold Mirels, and John L. Cummings

Lewis Flight Propulsion Laboratory
Cleveland, Ohio

DISTRIBUTION STATEMENT A
Approved for Public Release
Distribution Unlimited



Washington

August 1950

Reproduced From
Best Available Copy

20000803 216

DTIC QUALITY INSPECTED 4

AQM00-10-3398

NATIONAL ADVISORY COMMITTEE FOR AERONAUTICS

TECHNICAL NOTE 2141

CHARTS FOR ESTIMATING DOWNWASH BEHIND
RECTANGULAR, TRAPEZOIDAL, AND TRIANGULAR
WINGS AT SUPERSONIC SPEEDS

By Rudolph C. Haefeli, Harold Mirels
and John L. Cummings

SUMMARY

Charts are presented for estimating the downwash behind wings in a supersonic stream. The wing plan forms for which computations are made include rectangular wings with reduced aspect ratios (cotangent of Mach angle times aspect ratio) of 2, 4, 8, and 12; trapezoidal wings with reduced aspect ratios ranging from 2 to 12.8 and taper ratios of $1/2$ and $1/4$; and triangular wings with reduced aspect ratios of 8 and 12. All the wings have supersonic leading and trailing edges.

The charts are obtained on the basis of lifting-line theory. For each wing, charts of the downwash near the wing, the downwash in the Trefftz plane, and the spanwise distribution of loading are presented. The charts are applicable behind the wings in regions where the effect of the rolling up of the trailing vortex sheet is not excessive. The calculation of downwash farther downstream is briefly discussed.

A procedure is indicated to correct for the displacement and the distortion of the trailing vortex sheet. The downwash behind wings with flaps is briefly considered.

INTRODUCTION

Charts presented in reference 1 for the downwash behind wings at subsonic speeds have proved of great value to the aircraft designer. With the recent emphasis on high-speed flight, a similar series of charts for the downwash behind wings at supersonic speeds would be equally useful. A computational program was therefore undertaken at the NACA Lewis laboratory to provide such charts.

The downwash charts presented herein are based on the lifting-line theory of reference 2. Downwash results obtained from the linearized theory of reference 2 may differ from those encountered in practice due to (from references 1 and 3):

1. Displacement and distortion of the trailing vortex sheet
2. Differences between theoretical and actual spanwise distribution of loading
3. Wing-body interference
4. Viscous-wake effects

A first-order correction for the displacement and the distortion of the trailing vortex sheet, as suggested in reference 1, is incorporated. The region of validity of this approximation is discussed on the basis of the analysis of reference 4.

Charts are presented for obtaining the downwash behind rectangular, trapezoidal, and triangular wings, all of which have supersonic leading and trailing edges. The downwash behind triangular wings with subsonic leading edges is presented in references 5 and 6.

THEORY

Downwash Near Wing

The vertical perturbation velocity at a point x, y, z induced by a lifting line lying in the $z = 0$ plane along the y -axis (fig. 1(a)) is given in reference 2 (equation (46)) as

$$w = -\frac{1}{2\pi} \int_{y_a}^{y_b} \frac{x(y-y_0)(r_0^2 - \beta^2 z^2)}{r_0(x^2 - \beta^2 z^2) [(y-y_0)^2 + z^2]} \frac{d\Gamma}{dy_0} dy_0 \quad (1)$$

where Γ is the spanwise distribution of circulation and y_a and y_b are the ordinate limits of the lifting line contained within the forward Mach cone from x, y, z . (The main symbols used in this report are defined in appendix A.) The integration may be

approximated by a summation corresponding to replacing the lifting line and its shed vortex sheet by a finite number of horseshoe vortices. That is, a smooth spanwise variation in circulation is replaced by a stepwise variation, as illustrated in figure 1(b). Equation (1) then becomes

$$w = - \frac{1}{2\pi} \sum_{i=1}^n \frac{x(y-y_i)(r_i^2 - \beta^2 z^2)}{r_i(x^2 - \beta^2 z^2) [(y-y_i)^2 + z^2]} (\Delta\Gamma)_i \quad (2)$$

where $(\Delta\Gamma)_i$ is the strength of the i -th trailing line vortex, y_i is the spanwise coordinate of the i -th trailing line vortex, and n is twice the number of horseshoe vortices used. The terms for which r_i is imaginary are omitted from the summation because such terms arise from line vortices that lie outside the forecone from x, y, z . This summation corresponds to integrating equation (1) between the limits y_a and y_b . The sign of $(\Delta\Gamma)_i$ is negative if, by applying the right-hand rule, the vortex vector is in the positive x -direction. The magnitude of $(\Delta\Gamma)_i$ is equal to the jump of the i -th step in the load distribution.

Equation (2) may be put in a form more suitable for computations by substituting $\xi = x/\beta b'$, $\eta = y/b'$, and $\zeta = z/b'$ to obtain

$$w = - \frac{1}{2\pi} \sum_{i=1}^n \frac{\xi(\eta-\eta_i) [\xi^2 - (\eta-\eta_i)^2 - 2\zeta^2]}{\sqrt{\xi^2 - (\eta-\eta_i)^2 - \zeta^2} (\xi^2 - \zeta^2) [(\eta-\eta_i)^2 + \zeta^2]} \frac{(\Delta\Gamma)_i}{b'} \\ = - \frac{1}{2\pi} \sum_{i=1}^n G_i \frac{(\Delta\Gamma)_i}{b'} \quad (3)$$

Flat-plate wings will be assumed for the remainder of the report. The results are applicable to other wings, however, inasmuch as the downwash behind a wing with thickness and camber equals the flat-plate solution plus the downwash of the wing at zero angle of attack. Thus,

$$\frac{w}{\alpha U} = - \frac{d\epsilon}{d\alpha} + \frac{w_{\alpha=0}}{\alpha U}$$

where $w_{\alpha=0}$ is the downwash of the wing at zero angle of attack. For a flat plate,

$$\frac{w}{\alpha U} = - \frac{d\epsilon}{d\alpha}$$

so that equation (3) may be written as

$$\frac{d\epsilon}{d\alpha} = \frac{1}{2\pi} \frac{\Gamma_m}{\alpha U b'} \sum_{i=1}^n G_i \frac{(\Delta\Gamma)_i}{\Gamma_m} \quad (4)$$

where Γ_m is the value of Γ at midspan.

The factor G_i is singular for points on a line vortex; that is, when $\eta = \eta_i$ and $\xi = 0$. Comparison of downwash obtained by analytic integration and numerical integration indicates that the computational points in the $\xi = 0$ plane should be half-way between line vortices when equation (4) is used. Computational points, with $\xi \neq 0$, that lie on the aftercone from a corner of a horseshoe vortex should be avoided inasmuch as the radical in the denominator of G_i is then zero.

The results of reference 2 show that the lifting-line approximation gives values of downwash that are in good agreement with the exact linearized solution if the lifting line is placed at the 1/2-chord point for rectangular wings and at the 3/4-chord point for triangular wings. For the present computations, the line vortices were therefore placed at these chordwise locations. The 1/2-chord location was also used for the trapezoidal wings.

Near the trailing edge of a wing the lifting-line method is not in close agreement with exact linearized theory. At the trailing edge, however, the exact linearized value of the downwash may be readily obtained by the methods of reference 7. For trailing edges normal to the free-stream direction, this method yields

$$\frac{d\epsilon}{d\alpha} = 1 - \frac{\beta u}{\alpha U} \quad (5)$$

where u is the perturbation velocity in the x -direction on the top surface of the wing at the trailing edge. An estimate of the downwash near the trailing edge in the $z = 0$ plane may then be

made by fairing the curve obtained by the line-vortex method (equation (4)) to the value at the trailing edge given by equation (5).

Displacement and Distortion of Vortex Sheet

Methods for calculating the effect of distortion on the downwash are discussed in references 1, 4, and 8. In linearized theory, the trailing vortex sheet is ordinarily assumed to lie in the $z = 0$ plane. Actually, the trailing vortex sheet is displaced and distorted by the perturbation velocities and generally tends to roll up at the edges. The rolling-up process continues until the entire vorticity is concentrated in two vortex cores trailing behind each wing tip.

The distance behind the trailing edge at which the vortex sheet is essentially rolled up is (reference 4), in the reduced coordinate system,

$$\frac{e}{\beta b'} = 2K \frac{A}{C_L} \quad (6)$$

where K is a factor dependent on the load distribution. For elliptical load distributions, $K \approx 0.28$, whereas for distributions that have a lateral center of lift farther outboard, K takes on smaller values, and vice versa. The distance e is directly proportional to A/C_L .

At downstream stations for which $x/\beta b' < (e+c)/\beta b'$, both the displacement and the distortion of the trailing vortex sheet are considered adequately accounted for when computing downwash near the plane of symmetry ($y/b' = 0$) by assuming the vortex sheet to be displaced as a unit (that is, undistorted) at each downstream station by the amount of local displacement of the center line of the actual vortex sheet. The downward displacement of the center line of the vortex sheet from the trailing edge may be estimated by integrating the linearized downwash along that line. Thus, the total downward displacement from the $z = 0$ plane is

$$\begin{aligned} h &= h_t + h_s \\ &= c\alpha + \alpha \int_{x_t}^{x_l} \frac{d\epsilon}{d\alpha} dx \end{aligned} \quad (7)$$

where $h_t = c\alpha$ is the downward displacement of the trailing edge from the $z = 0$ plane with coordinate origin at the leading edge,

and $h_s = \alpha \int_{x_t}^{x_1} \frac{d\epsilon}{d\alpha} dx$ is the downward displacement of the vortex sheet from the trailing edge at a downstream station x_1 .

The downwash at stations for which $x/\beta b' > (e+c)/\beta b'$ is essentially simpler to calculate. A procedure applicable for these stations is indicated in appendix B. The emphasis of this report is on the calculation of downwash near the wing, where the calculation is more difficult.

The distance e cannot be accurately determined at present because of insufficient knowledge about the factor K . Ultimately, the magnitude of K must be experimentally determined for various plan forms.

Downwash in Trefftz Plane

In the Trefftz plane ($x/\beta b' = \infty$), equation (4) reduces to

$$\frac{d\epsilon}{d\alpha} = \frac{1}{2\pi} \frac{\Gamma_m}{\alpha U b'} \sum_{i=1}^n \frac{\eta - \eta_i}{(\eta - \eta_i)^2 + \xi^2} \frac{(\Delta\Gamma)_i}{\Gamma_m} \quad (8)$$

Equation (8) is identical to the equation obtained in subsonic theory for the downwash at $x = \infty$.

Because of the displacement and the distortion of the trailing vortex sheet and its ultimate degeneration into two trailing vortex cores, the Trefftz plane solution is not a correct approximation to the actual downwash an infinite distance behind a wing. The Trefftz plane solution is nevertheless useful for estimating the magnitude and the spanwise variation of downwash at downstream stations for which asymptotic values of downwash are approached before $x/\beta b'$ exceeds $(e+c)/\beta b'$. This condition, however, may not be obtained for wings with either a small aspect ratio or a large lift coefficient.

Spanwise Distribution of Loading

Analytical expressions for the potential jump $\Delta\phi$ across the plane of each wing were obtained by the method of reference 9. These equations are given in appendix C for the wing regions considered in this report. The spanwise variation in loading was obtained with the relation $\Gamma = (\Delta\phi)_t$. The lift coefficient for the trapezoidal wings was obtained by a graphical integration of the spanwise loading curves. For the triangular wings, $C_L = \frac{4\alpha}{\beta}$

(reference 10, p. 361), and for the rectangular wings, $C_L = \frac{4\alpha}{\beta} \left(1 - \frac{1}{2\beta A}\right)$ (reference 10, p. 380).

Downwash Due to Flaps

The contribution of wing flaps of constant chord to the vertical perturbation velocity may be approximated by replacing the flap by a horseshoe vortex (fig. 2) with strength equal to the circulation of a two-dimensional airfoil of the same chord. That is, (from equation (C1))

$$\Gamma_f = \frac{2m_t \xi_f}{\sqrt{m_t^2 - 1}} \delta U b' \quad (9)$$

where m_t is the slope parameter of the trailing edge, δ is the flap deflection angle, and ξ_f is the chord parameter of the flap (δ and ξ_f are measured in the flight direction). From equation (3), the downwash due to both flaps is

$$-\frac{w}{\delta U} = \frac{1}{2\pi} \frac{\Gamma_f}{\delta U b'} \frac{(\xi - \xi')}{[(\xi - \xi')^2 - \zeta^2]} \left\{ \frac{(\eta - \eta_1) [(\xi - \xi')^2 - (\eta - \eta_1)^2 - 2\zeta^2]}{\sqrt{(\xi - \xi')^2 - (\eta - \eta_1)^2 - \zeta^2} [(\eta - \eta_1)^2 + \zeta^2]} - \right. \\ \frac{(\eta - \eta_2) [(\xi - \xi')^2 - (\eta - \eta_2)^2 - 2\zeta^2]}{\sqrt{(\xi - \xi')^2 - (\eta - \eta_2)^2 - \zeta^2} [(\eta - \eta_2)^2 + \zeta^2]} + \frac{(\eta + \eta_2) [(\xi - \xi')^2 - (\eta + \eta_2)^2 - 2\zeta^2]}{\sqrt{(\xi - \xi')^2 - (\eta + \eta_2)^2 - \zeta^2} [(\eta + \eta_2)^2 + \zeta^2]} - \\ \left. \frac{(\eta + \eta_1) [(\xi - \xi')^2 - (\eta + \eta_1)^2 - 2\zeta^2]}{\sqrt{(\xi - \xi')^2 - (\eta + \eta_1)^2 - \zeta^2} [(\eta + \eta_1)^2 + \zeta^2]} \right\}$$

where ξ' is the distance (in the nondimensional coordinate system) of the horseshoe vortex from the y, η -axis, and $\pm\eta_1$ and $\pm\eta_2$ are the nondimensional ordinates of the trailing line vortices. This downwash is then added to the downwash of the plain wing, as indicated in figure 2, to obtain the downwash due to the complete wing configuration.

This approximation should result in a good indication of the downwash if the flap deflection δ is small, and if the flap chord is small compared with the wing chord. For computations of the downwash close to the trailing edge, additional refinements to correct for the effect of the chordwise distribution of vorticity may be required.

DISCUSSION OF DOWNWASH CHARTS

Scope of Charts

The wing plan forms for which the downwash was computed, together with an index to the charts (figs. 3 to 22), are shown in table I. The plan forms include rectangular wings with reduced aspect ratios βA of 2, 4, 8, and 12; trapezoidal wings with reduced aspect ratios ranging from 2 to 12.8 and taper ratios of $1/2$ and $1/4$; and triangular wings with reduced aspect ratios of 8 and 12. The wings are assumed to be flat plates with the specified plan form.

Those plan forms having swept trailing edges are modified at the midspan by parabolic arcs, tangent to the trailing edges at $0.2b'$, in order to decrease the magnitudes of downwash in the vicinity of the midspan. (For these wings, linearized theory predicts both a discontinuity in the slope of the spanwise loading curve and an infinite vertical perturbation velocity at the midspan (reference 2), neither of which would be expected in an actual fluid flow.) The reduced aspect ratios and taper ratios of the trapezoidal wing, however, are based on the original plan form.

The downwash charts obtained from equation (4) are presented in figures 3 to 22 for each plan form of table I for $y/b' = 0, 0.15$, and 0.30 , and $|z/b'| = 0, 0.1, 0.3$, and 0.5 . A coordinate origin at the midspan of the leading edge was chosen for the presentation of the charts.

Nineteen horseshoe vortices ($n = 38$) were used in equations (4) and (8) to calculate the downwash because trial computations indicated that this number was sufficiently large to yield good agreement with equation (1), yet not excessively large for practical computation.

Equation (5) was used to obtain values of $dc/d\alpha$ at the mid-span of the trailing edge of each wing. Curves were then drawn, indicated by the dashed lines in the downwash charts, to approximate the downwash in the regions close behind the trailing edges. These approximations were used for the calculations of the vortex-sheet displacement curves (by equation (7)), which appear on each chart.

The charts also present curves of the downwash in the Trefftz plane obtained from equation (8) for $|z/b'| = 0, 0.1, 0.3$, and 0.5 . These curves provide a basis for extrapolating downwash near the wing for $y/b' > 0.30$. The spanwise load distribution of each wing is also presented.

Comparisons with Exact Linearized Theory

Exact linearized values of downwash behind the rectangular wings of figures 19 to 22, obtained by the method of reference 7, illustrate the good agreement obtained by the lifting-line solutions for $z/b' = 0$ and $x/\beta b' > c/\beta b' + 1/2$. In the Trefftz plane, exact linearized values of downwash (taken from references 7 and 11) are shown for the triangular wings in figures 3 and 4 and for the rectangular wings in figures 19 to 22. Because discontinuities in the slopes of the downwash curves are not accurately predicted by the approximation of equation (4), the spanwise variation of downwash in the Trefftz plane deviates from the exact linearized values near the coordinates of such discontinuities. (See, for example, figs. 20 and 22.) The agreement is generally good, however. On the basis of these comparisons and the results of reference 2, all the downwash charts are believed to approximate closely exact linearized theory.

Factors Influencing Downwash

Magnitude of downwash. - A comparison of the downwash near the wing with the downwash in the Trefftz plane for the various plan forms considered indicates that the values of downwash in the Trefftz plane may be assumed to yield good estimates of the order

of magnitude of the downwash at stations for which $x/\beta b' > 2$. The downwash in the Trefftz plane at $y/b' = 0$ and $z/b' = 0$ may be expressed for particular load distributions in terms of the lift coefficient and the aspect ratio. Thus, for a uniform load distribution (reference 12, p. 134),

$$\frac{d\epsilon}{d\alpha} = \frac{\frac{C_L}{\alpha}}{\pi A} \quad (10)$$

whereas, for an elliptic load distribution (reference 12, p. 143),

$$\frac{d\epsilon}{d\alpha} = 2 \frac{\frac{C_L}{\alpha}}{\pi A} \quad (11)$$

In general,

$$\frac{d\epsilon}{d\alpha} = p \frac{\frac{C_L}{\alpha}}{\pi A} \quad (12)$$

where p is a number dependent on the particular load distribution.

For loadings ranging between the uniform and the elliptic distributions, $1 < p < 2$; whereas for loadings ranging between the elliptic and triangular distributions, $p > 2$. In general, the order of magnitude of the downwash is therefore directly proportional to the lift coefficient and a factor dependent on the form of the load distribution curve, and inversely proportional to the aspect ratio.

Spanwise variation of downwash. - The spanwise variation of downwash in the $z = 0$ plane is directly related to the form of the load-distribution curve. The effect of the load distribution on downwash is illustrated in figure 23. This figure presents the downwash in the Trefftz plane, for $z = 0$, behind triangular, elliptical, and uniform load distributions.

For triangular loading (fig. 23(a)), the downwash in the $z = 0$ plane approaches infinity at midspan. If the load distribution is modified so that zero slope exists at midspan, however, a finite, maximum downwash results (figs. 3 and 4). A greater modification of the triangular loading may further decrease the

downwash at midspan so that the maximum occurs at another spanwise station (for example, near $y/b' = 0.15$, fig. 5). The basic characteristic of the triangular-type loading, however, is the decrease in $d\epsilon/d\alpha$ behind the wing with an increase in y .

The basic characteristic of elliptic loading (fig. 23(b)) and modifications thereof (fig. 10) is the essentially constant spanwise downwash distribution behind the wing. For uniform loading (fig. 23(c)) and modifications of uniform loading (fig. 21) the downwash parameter $d\epsilon/d\alpha$ increases with y .

Above the plane of the wing, the load distribution does not have as pronounced an effect on the spanwise variation of downwash as it has in the $z = 0$ plane.

Displacement Curves

The displacement curves indicate that the displacement is practically negligible for $x/\beta b' < 2$ when α and β have values consistent with linearized theory. Farther downstream, the displacement increases practically linearly with distance.

METHOD OF APPLICATION

The downwash parameter $d\epsilon/d\alpha$ at a point behind a wing is obtained from the charts given in figures 3 to 22 as follows:

1. For a Mach number under consideration, the coordinates of the point where the downwash is desired are reduced to the parameters $x/\beta b'$, y/b' , and z/b' measured from an origin at the midspan of the leading edge.
2. At stations near the plane of symmetry ($y/b' = 0$), the displacement h/b' of the vortex sheet from the $z = 0$ plane is estimated from the displacement chart. This value is added to z/b' to obtain the net distance of the point from the vortex sheet.
3. For the $x/\beta b'$ and y/b' parameters of the point, and the net z/b' parameter found in step 2, the value of $d\epsilon/d\alpha$ is obtained from the downwash charts.

If the magnitude of the downwash w is desired, the relations

$$w = - \frac{d\epsilon}{d\alpha} \alpha U + w_{\alpha=0} \quad \text{for wings with thickness and camber}$$

and

$$w = - \frac{d\epsilon}{d\alpha} \alpha U \quad \text{for flat plates}$$

1324

may be used, where $w_{\alpha=0}$ is the downwash of the wing at zero angle of attack. For wings with flaps, the computation indicated in the section Downwash Due to Flaps must also be made.

A correction for the downwash based on an experimental lift coefficient is discussed in appendix D. For wings with a small value of A/C_L , the rolling up of the trailing vortex sheet must be considered, as indicated in appendix B.

EXAMPLE

As an illustrative example, the downwash parameter $d\epsilon/d\alpha$ will be found at the point p ($x = 15.0$, $y = 1.5$, and $z = 1.0$) (fig. 24) behind a rectangular wing, assuming:

$$\beta A = 4$$

$$b' = 5.0$$

$$\alpha = 0.07 \text{ radians } (4^\circ)$$

$$M = 2$$

From the steps previously outlined there result:

$$1. \quad \beta = 1.73$$

$$x/\beta b' = 1.73$$

$$y/b' = 0.30$$

$$z/b' = 0.20$$

2. From figure 20

$$h/b' = 0.64 \alpha\beta = 0.08$$

The net vertical distance (nondimensional) of the point above the vortex sheet is then

$$(z/b')_{\text{net}} = 0.20 + 0.08 = 0.28$$

3. The value $d\epsilon/d\alpha = 0.27$ is the desired result.

Lewis Flight Propulsion Laboratory,
National Advisory Committee for Aeronautics,
Cleveland, Ohio, January 9, 1950.

APPENDIX A

SYMBOLS

The following symbols are used in this report:

A aspect ratio, $(2b')^2/S$

b' wing semispan

C_L lift coefficient, $L/(\frac{\rho}{2} U^2 S)$

c root chord

e distance from trailing edge to station where trailing vortex sheet is essentially rolled up

$$G_1 = \frac{\xi(\eta - \eta_1) [\xi^2 - (\eta - \eta_1)^2 - 2\xi^2]}{\sqrt{\xi^2 - (\eta - \eta_1)^2 - \xi^2} (\xi^2 - \xi^2) [(\eta - \eta_1)^2 + \xi^2]}$$

h downward displacement of trailing vortex sheet from $z = 0$ plane

h_s downward displacement of trailing vortex sheet from trailing edge

L lift

M free-stream Mach number

m_l slope of plan-form leading edge, $d\eta_l/d\xi_l$

m_t slope of plan-form trailing edge, $d\eta_t/d\xi_t$

n total number of trailing line vortices

$$r_i = \sqrt{x^2 - \beta^2(y - y_i)^2 - \beta^2 z^2}$$

$$r_o = \sqrt{x^2 - \beta^2(y - y_o)^2 - \beta^2 z^2}$$

S plan-form area

T taper ratio, tip chord divided by root chord

U free-stream velocity (taken in x-direction)

$\left. \begin{array}{l} u \\ v \\ w \end{array} \right\}$ perturbation velocities in directions x,y,z, respectively

$\left. \begin{array}{l} x \\ y \\ z \end{array} \right\}$ Cartesian coordinate system

α angle of attack, radians

β cotangent of Mach angle, $\sqrt{M^2-1}$

βA reduced aspect ratio

Γ spanwise distribution of circulation

$\Delta\Gamma$ strength of line vortex

δ flap deflection angle, radians

ϵ downwash angle, radians (positive for downward flow deflection)

$\xi = x/\beta b'$

$\eta = y/b'$

$\zeta = z/b'$

ρ free-stream density

φ perturbation-velocity potential

$\Delta\varphi$ potential jump across $z = 0$ plane ($\varphi_{\text{top}} - \varphi_{\text{bottom}}$)

Subscripts:

f flap

$i = 1, 2, 3, \dots, n$ line vortices

l plan-form leading edge

m value at midspan

o variable of integration

t plan-form trailing edge

APPENDIX B

DOWNWASH AT STATIONS WHERE VORTEX SHEET

IS ESSENTIALLY ROLLED UP

At stations for which $x/\beta b' > (e+c)/\beta b'$, an approximation to the downwash may be obtained by representing the wing by a single horseshoe vortex, the strength of which is equal to Γ_m and the span of which is such that the net lift of the horseshoe vortex equals that of the wing. The corresponding semispan, given by

$$\eta_1 = \int_0^1 \frac{\Gamma(\eta_0)}{\Gamma_m} d\eta_0, \text{ is indicated in each loading chart of fig-}$$

ures 3 to 22 by a vertical long-short dashed line. The downwash, then, is (from equation (8))

$$\frac{d\epsilon}{d\alpha} = \frac{1}{2\pi} \frac{\Gamma_m}{\alpha U b'} \left[\frac{\eta - \eta_1}{(\eta - \eta_1)^2 + \zeta^2} + \frac{\eta + \eta_1}{(\eta + \eta_1)^2 + \zeta^2} \right]$$

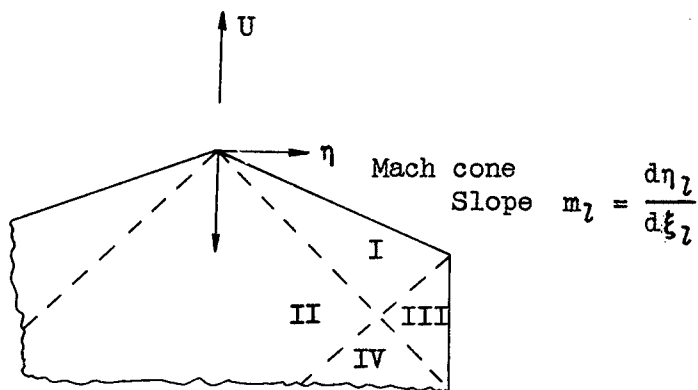
An estimate of the displacement of the trailing line vortices from the $z = 0$ plane may be obtained by computing the downwash parameter at $\eta = \eta_1$, $\zeta = 0$ due to the line vortex at $\eta = -\eta_1$ and assuming that this value of $d\epsilon/d\alpha$ is constant from the trailing edge to the station at which the displacement is being computed (reference 3). Thus, the displacement is

$$h = c\alpha + \frac{\Gamma_m}{\alpha U b'} \frac{\alpha(x-c)}{4\pi\eta_1}$$

APPENDIX C

SPANWISE DISTRIBUTION OF CIRCULATION

The spanwise distribution of circulation was obtained by evaluating the following equations for $\Delta\varphi$ along the trailing edge of each wing; that is, $\Gamma = (\Delta\varphi)_t$: These equations were obtained by the method of reference 9.



Region I

$$\frac{\Delta\varphi}{\alpha U} = \frac{2b'(m_2\xi - \eta)}{\sqrt{m_2^2 - 1}} \quad (C1)$$

Region II

$$\frac{\Delta\varphi}{\alpha U} = \frac{4b'}{\pi\sqrt{m_2^2 - 1}} \left[(m_2\xi - \eta) \tan^{-1} \sqrt{\frac{(m_2 - 1)(\xi + \eta)}{(m_2 + 1)(\xi - \eta)}} + (m_2\xi + \eta) \tan^{-1} \sqrt{\frac{(m_2 - 1)(\xi - \eta)}{(m_2 + 1)(\xi + \eta)}} \right] \quad (C2)$$

Region III

$$\frac{\Delta\varphi}{\alpha U} = \frac{4b'}{\pi\sqrt{m_2^2 - 1}} \left\{ \sqrt{(1 - \eta)[m_2(\xi + \eta) - (m_2 + 1)]} + \frac{m_2\xi - \eta}{\sqrt{m_2 + 1}} \tan^{-1} \sqrt{\frac{(m_2 + 1)(1 - \eta)}{m_2(\xi + \eta) - (m_2 + 1)}} \right\} \quad (C3)$$

Region IV

$$\begin{aligned}
 \frac{\Delta\varphi}{\alpha U} = & \frac{4b'}{\pi\sqrt{m_2-1}} \left\{ \sqrt{(1-\eta) [m_2(\xi+\eta) - (m_2+1)]} + \right. \\
 & \frac{m_2\xi-\eta}{\sqrt{m_2+1}} \left[\tan^{-1} \sqrt{\frac{(m_2+1)(1-\eta)}{m_2(\xi+\eta) - (m_2+1)}} - \tan^{-1} \sqrt{\frac{(m_2+1)(\xi-\eta)}{(m_2-1)(\xi+\eta)}} \right] + \\
 & \left. \frac{m_2\xi+\eta}{\sqrt{m_2+1}} \tan^{-1} \sqrt{\frac{(m_2-1)(\xi-\eta)}{(m_2+1)(\xi+\eta)}} \right\} \quad (C4)
 \end{aligned}$$

APPENDIX D

CORRECTION BASED ON EXPERIMENTAL

LIFT DATA

Inasmuch as the change in downwash is proportional to the change in circulation and therefore to the change in lift, the ratio

$$\frac{(\partial C_L / \partial \alpha)_{\text{experimental}}}{(\partial C_L / \partial \alpha)_{\text{theoretical}}}$$

may be introduced as a correction factor for $d\epsilon/d\alpha$. This correction assumes that the form of the experimental loading curve is similar to the form of the theoretical loading curve. If the deviation of the experimental curve is large only near the wing tips, the correction factor should still yield satisfactory approximations to the downwash near midspan stations. Theoretical values of C_L/α are given in the charts.

For essentially flat plates, the ratio

$$\frac{C_{L\text{experimental}}}{C_{L\text{theoretical}}}$$

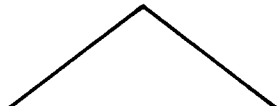
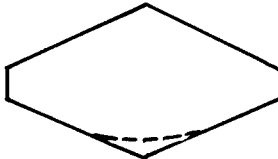
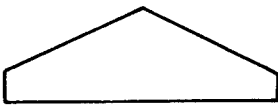

may be used as a correction factor for w .

REFERENCES

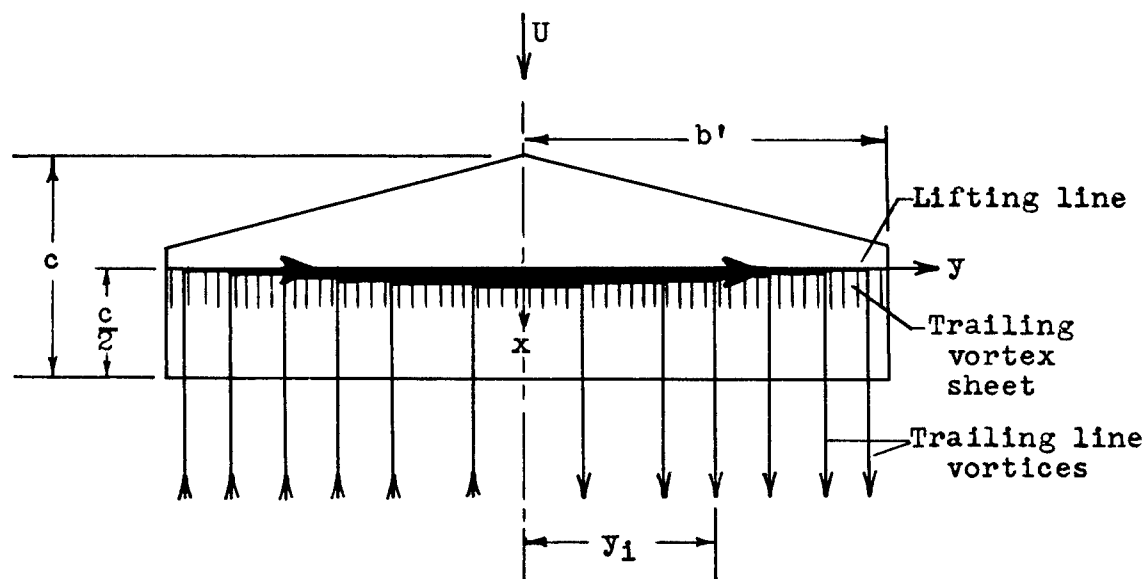
1. Silverstein, Abe, and Katzoff, S.: Design Charts for Predicting Downwash Angles and Wake Characteristics behind Plain and Flapped Wings. NACA Rep. 648, 1939.
2. Mirels, Harold, and Haefeli, Rudolph C.: Line-Vortex Theory for Calculation of Supersonic Downwash. NACA TN 1925, 1949.
3. Graham, Martha E.: Some Linearized Computations of Supersonic Wing-Tail Interference. Rep. No. SM-13430, Douglas Aircraft Co., Inc., Dec. 1948.

4. Spreiter, John R., and Sacks, Alvin H.: The Rolling Up of the Trailing Vortex Sheet and Its Effect on the Downwash behind Wings. I.A.S. Preprint No. 250, 1950.
5. Heaslet, Max A., and Lomax, Harvard: The Calculation of Downwash behind Supersonic Wings with an Application to Triangular Plan Forms. NACA TN 1620, 1948.
6. Lomax, Harvard, and Sluder, Loma: Downwash in the Vertical and Horizontal Planes of Symmetry behind a Triangular Wing in Supersonic Flow. NACA TN 1803, 1949.
7. Lagerstrom, P. A., and Graham, Martha E.: Downwash and Sidewash Induced by Three-Dimensional Lifting Wings in Supersonic Flow. Rep. No. SM-13007, Douglas Aircraft Co., Inc., April 1947.
8. Silverstein, Abe, Katzoff, S., and Bullivant, W. Kenneth: Downwash and Wake behind Plain and Flapped Airfoils. NACA Rep. 651, 1939.
9. Evvard, John C.: The Use of Source Distributions for Evaluating the Theoretical Aerodynamics of Thin Finite Wings at Supersonic Speeds. NACA Rep. 951, 1950.
10. Ferri, Antonio: Elements of Aerodynamics of Supersonic Flows. The MacMillan Co., 1949, pp. 361, 380.
11. Lagerstrom, P. A., and Graham, Martha E.: Methods for Calculating the Flow in the Trefftz-Plane behind Supersonic Wings. Rep. No. SM-13288, Douglas Aircraft Co., Inc., July 28, 1948.
12. Glauert, H.: The Elements of Aerofoil and Airscrew Theory. The MacMillan Co., 1944, pp. 134, 143.

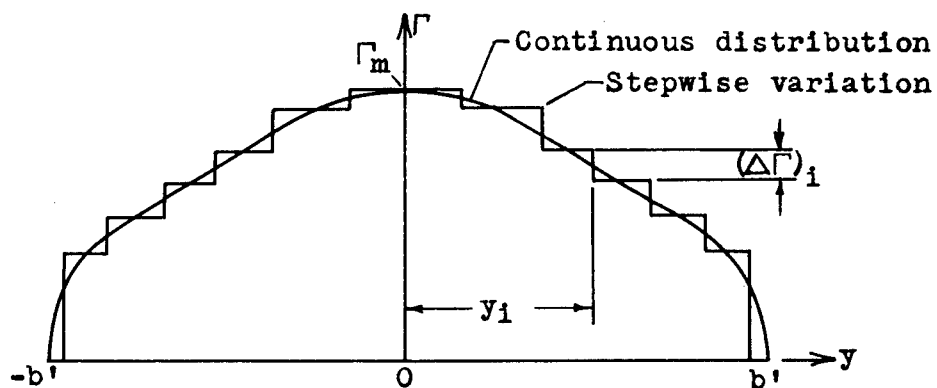
TABLE I. - PLAN FORMS AND INDEX TO CHARTS

Plan form	Figure	Reduced aspect ratio β_A	Taper ratio T
	3	8	0
	4	12	0
	5	2	1/4
	6	4	1/4
	7	8	1/4
	8	12	1/4
	9	2	1/2
	10	4	1/2
	11	8	1/2
	12	12	1/2
	13	3.2	1/4
	14	6.4	1/4
	15	12.8	1/4
	16	2.7	1/2
	17	5.3	1/2
	18	10.7	1/2
	19	2	1
	20	4	1
	21	8	1
	22	12	1





(a) Placement of trailing line vortices.



(b) Spanwise distribution of circulation.

Figure 1. - Lifting-line representation of wing.

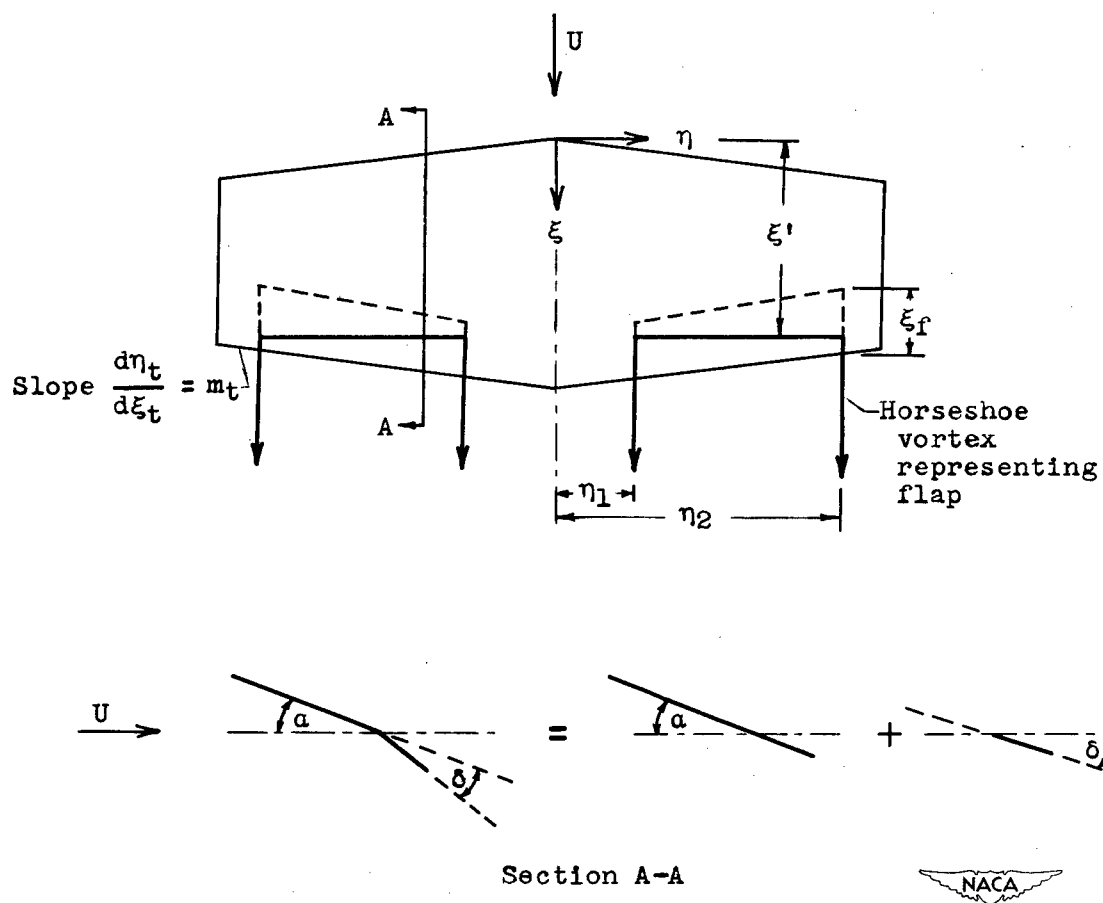
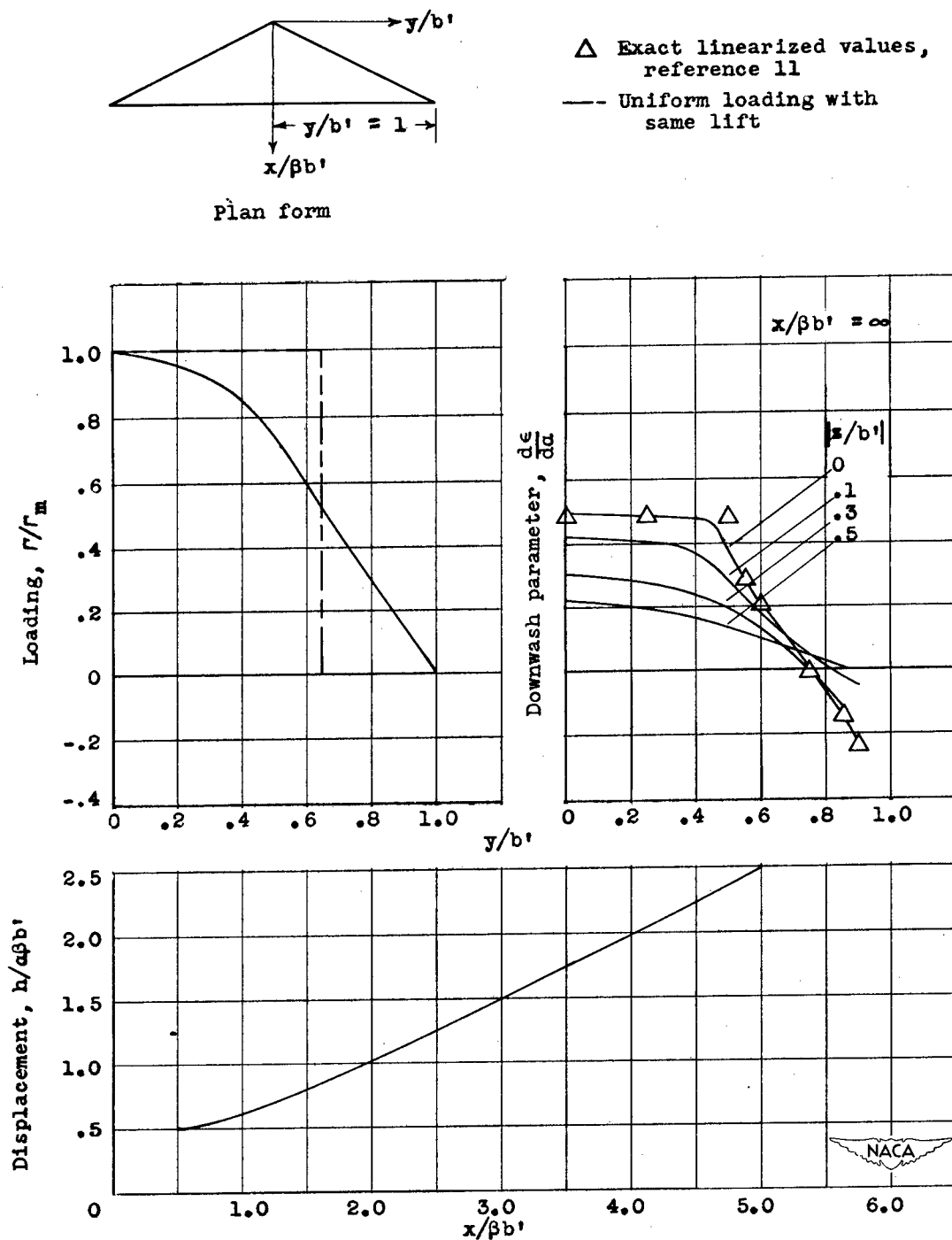
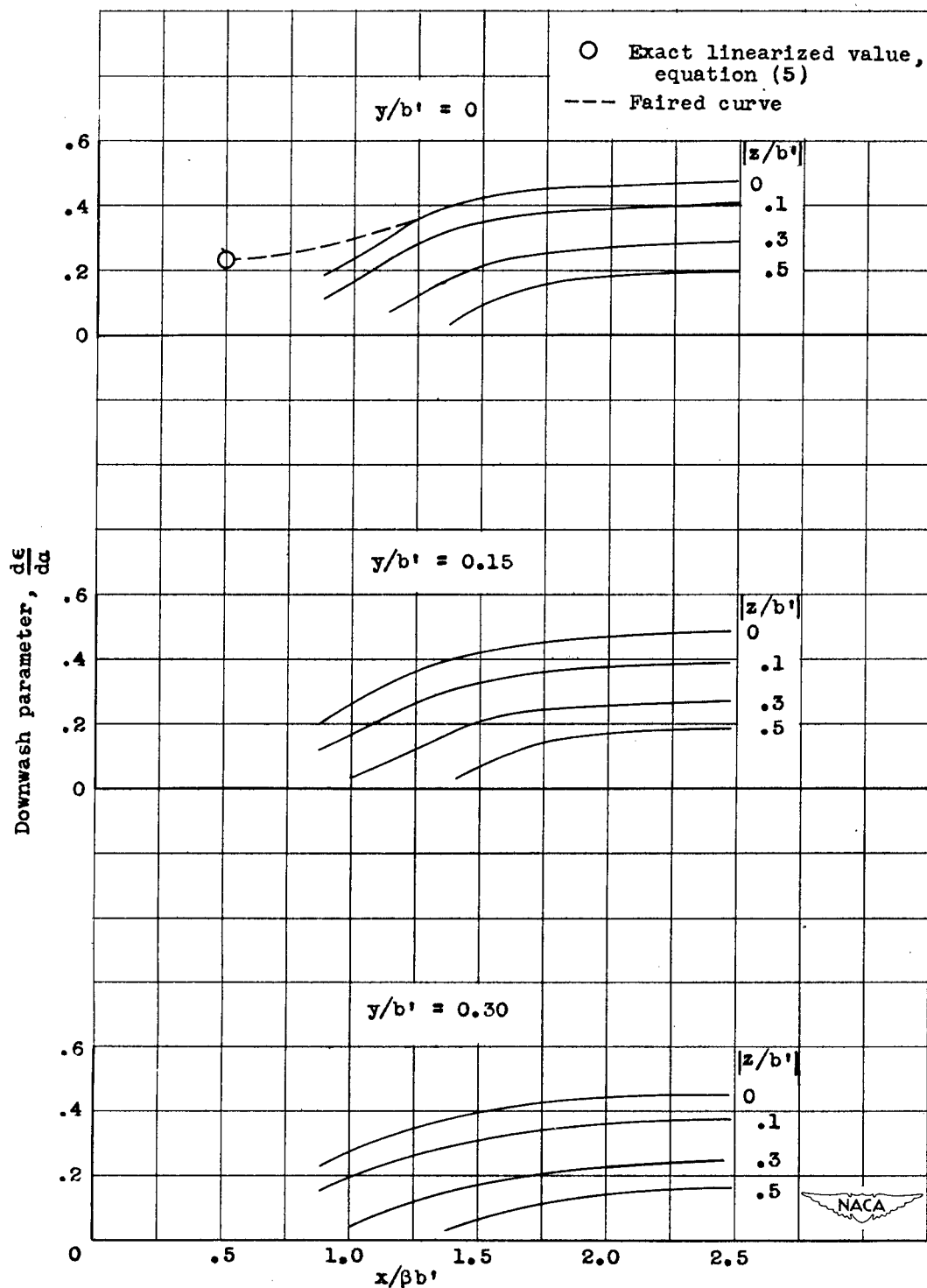


Figure 2. - Horseshoe-vortex representation of wing flaps.



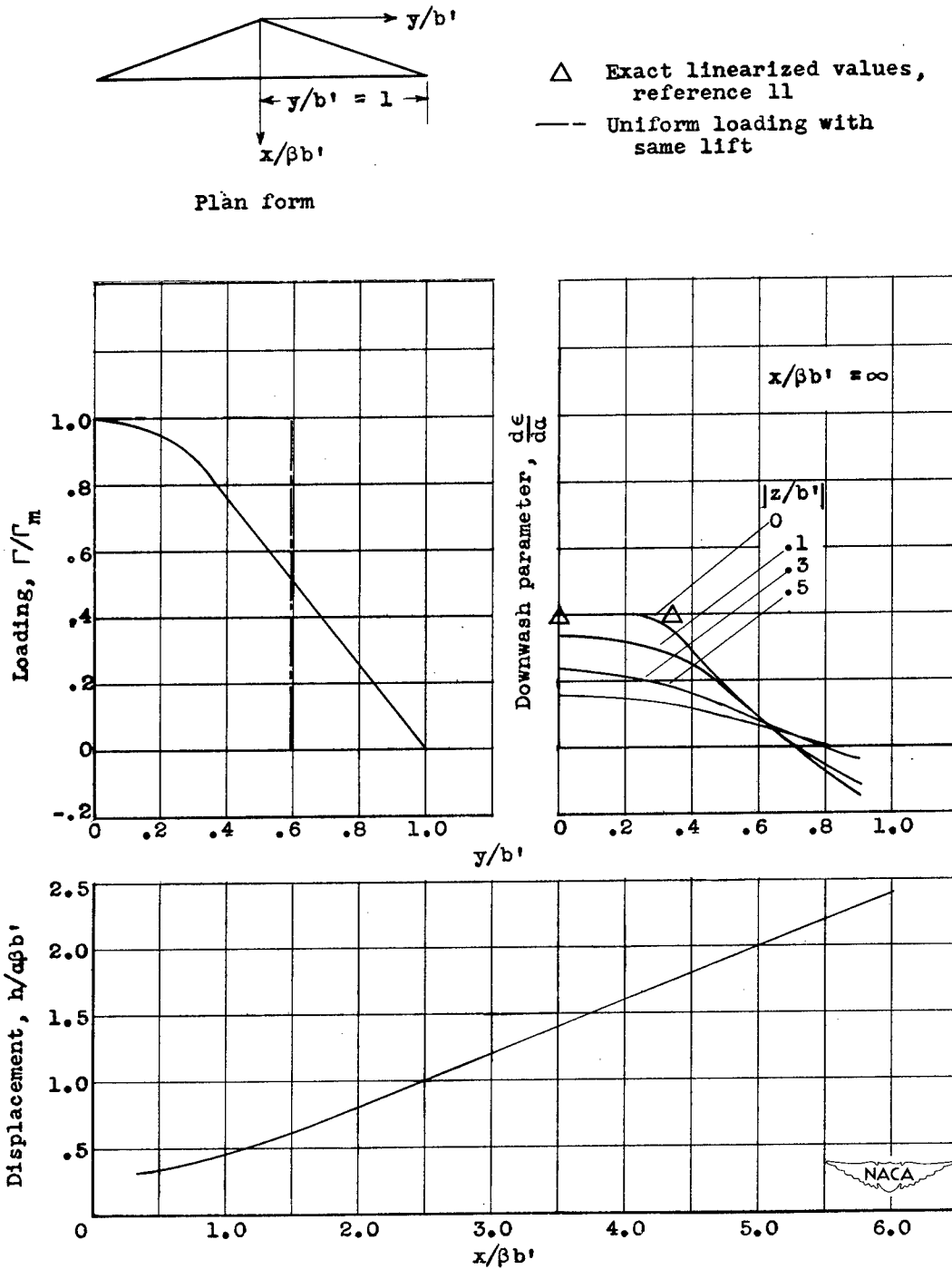
(a) Plan form, load distribution, downwash in Trefftz plane, and vortex-sheet displacement.

Figure 3. - Charts showing plan form, load distribution, downwash in Trefftz plane, vortex-sheet displacement, and downwash near wing. Reduced aspect ratio, 8; root chord, $0.500 \beta b'$; lift coefficient, $4.000 a/\beta$; midspan circulation, $0.770 aUb'$.



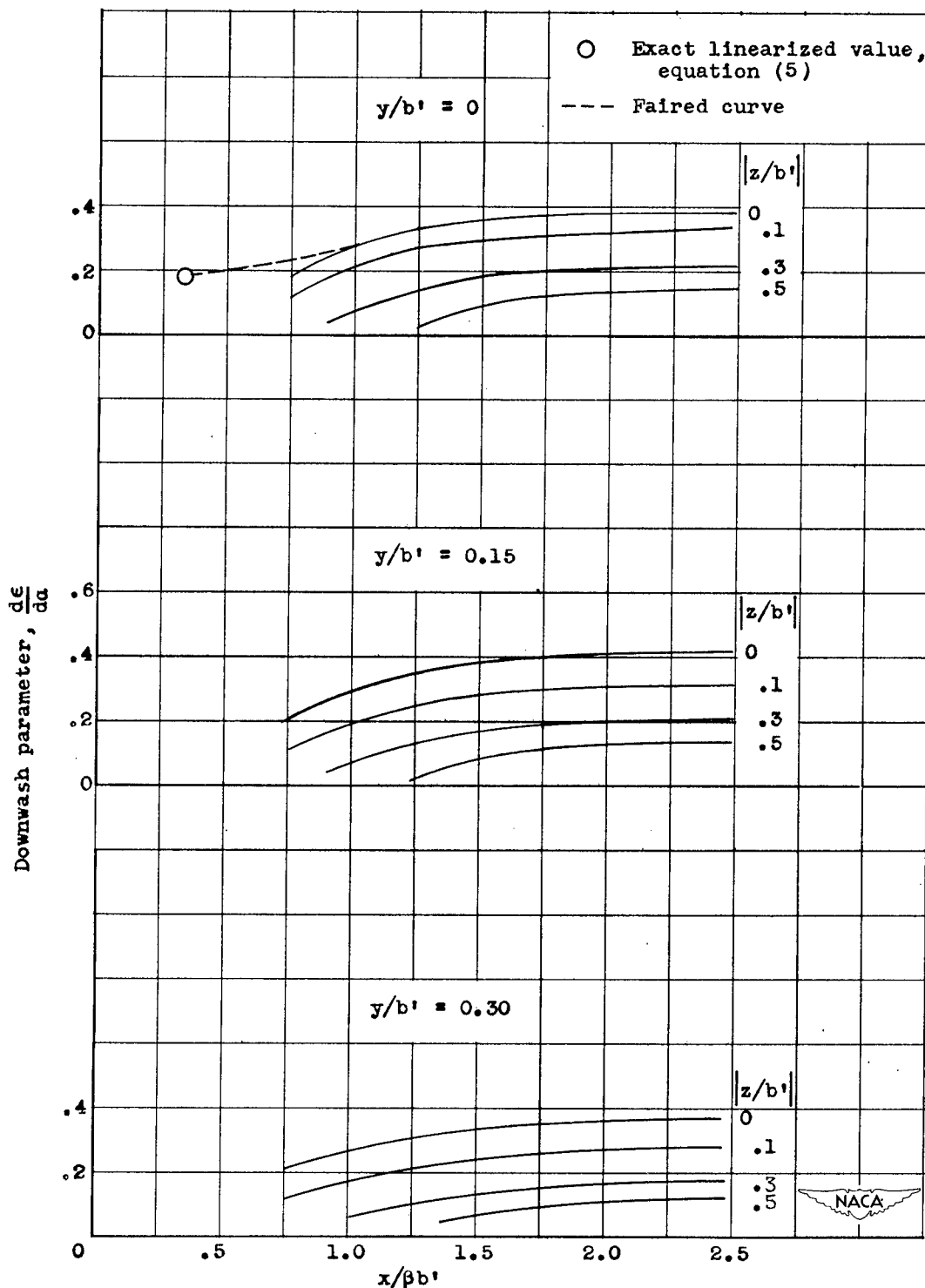
(b) Downwash near wing.

Figure 3. - Concluded. Charts showing plan form, load distribution, downwash in Trefftz plane, vortex-sheet displacement, and downwash near wing. Reduced aspect ratio, 8; root chord, $0.500 \beta b'$; lift coefficient, $4.000 \alpha/\beta$; midspan circulation, $0.770 \alpha U b'$.



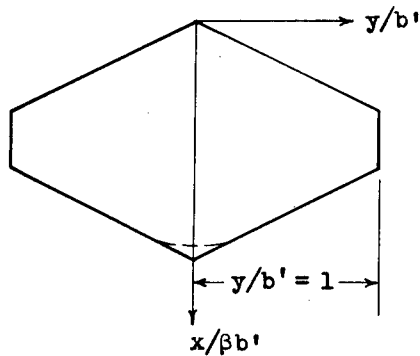
(a) Plan form, load distribution, downwash in Trefftz plane, and vortex-sheet displacement.

Figure 4. - Charts showing plan form, load distribution, downwash in Trefftz plane, vortex-sheet displacement, and downwash near wing. Reduced aspect ratio, 12; root chord, $0.333 \beta b'$; lift coefficient, $4.000 \alpha/\beta$; midspan circulation, $0.554 \alpha U b'$.



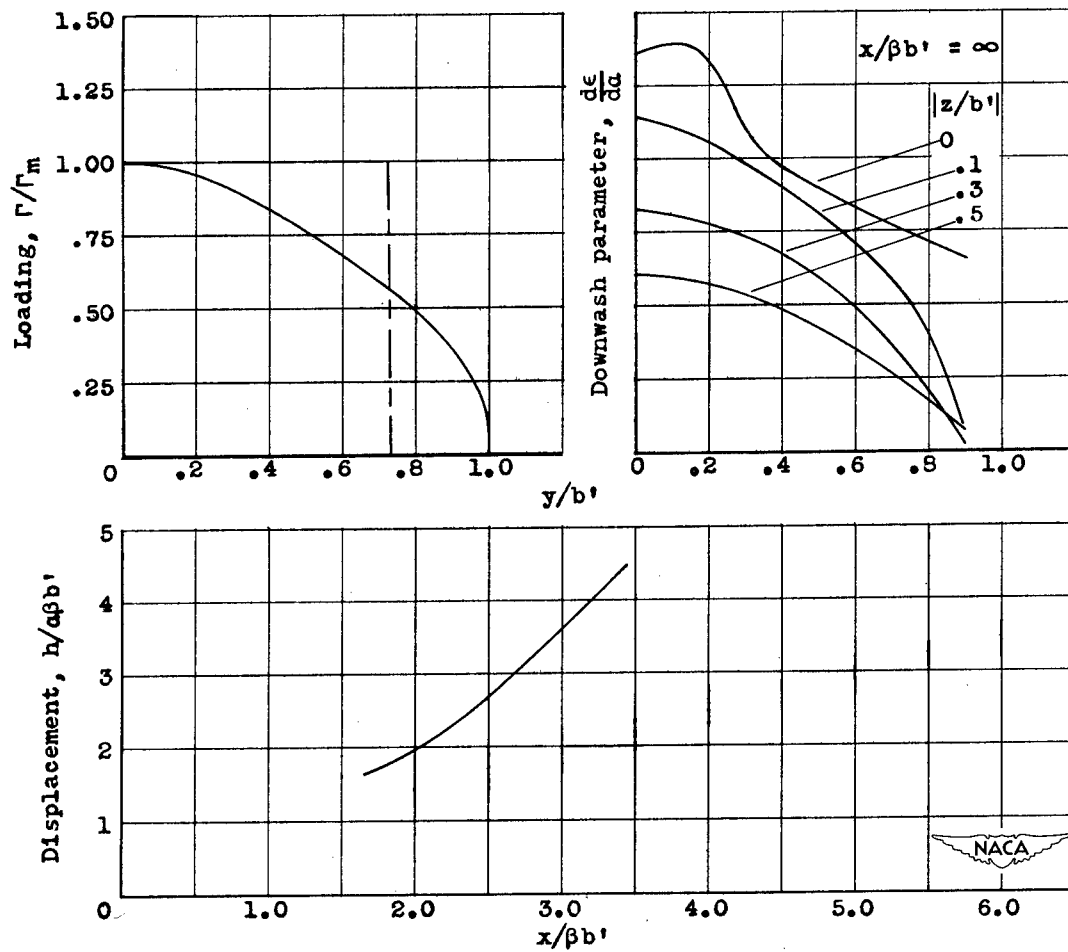
(b) Downwash near wing.

Figure 4. - Concluded. Charts showing plan form, load distribution, downwash in Trefftz plane, vortex-sheet displacement, and downwash near wing. Reduced aspect ratio, 12; root chord, $0.333 \beta b'$; lift coefficient, $4.000 a/\beta$; midspan circulation, $0.554 aUb'$.



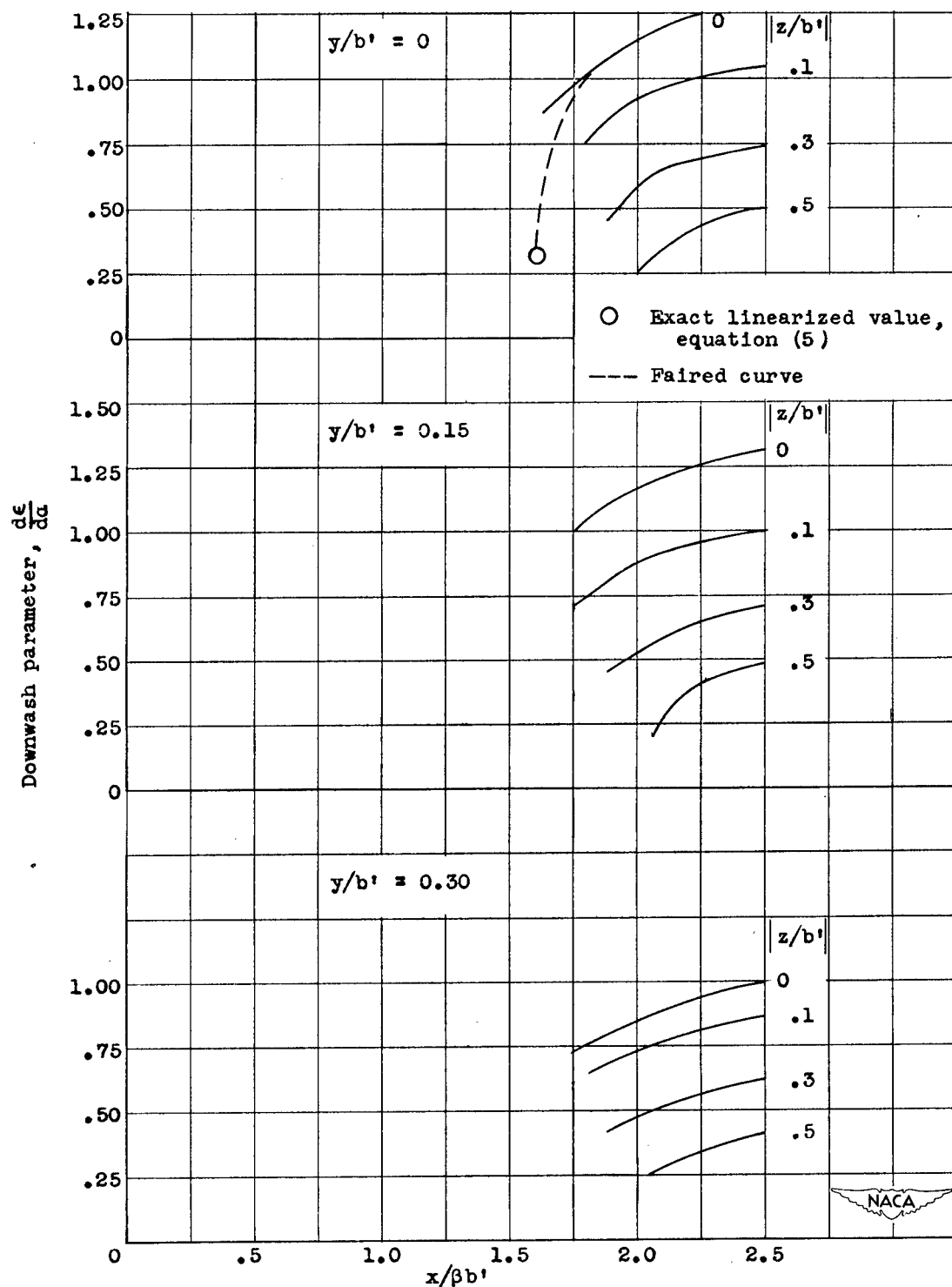
Plan form

----- Uniform loading
with same lift



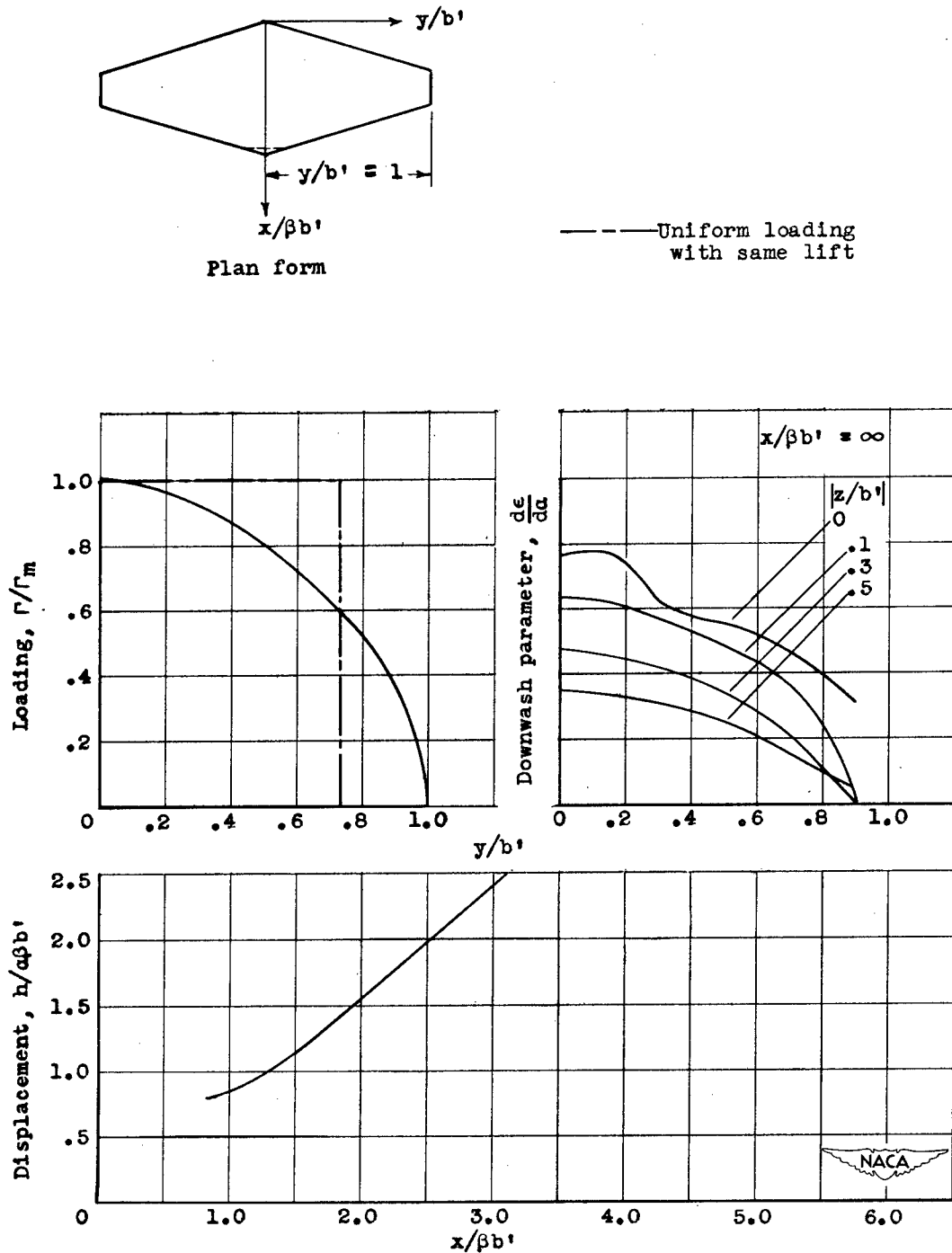
(a) Plan form, load distribution, downwash in Trefftz plane, and vortex-sheet displacement.

Figure 5. - Charts showing plan form, load distribution, downwash in Trefftz plane, vortex-sheet displacement, and downwash near wing. Reduced aspect ratio, 2; root chord, $1.600 \beta b'$; lift coefficient, $3.25 a/\beta$; midspan circulation, $2.273 aUb'$.



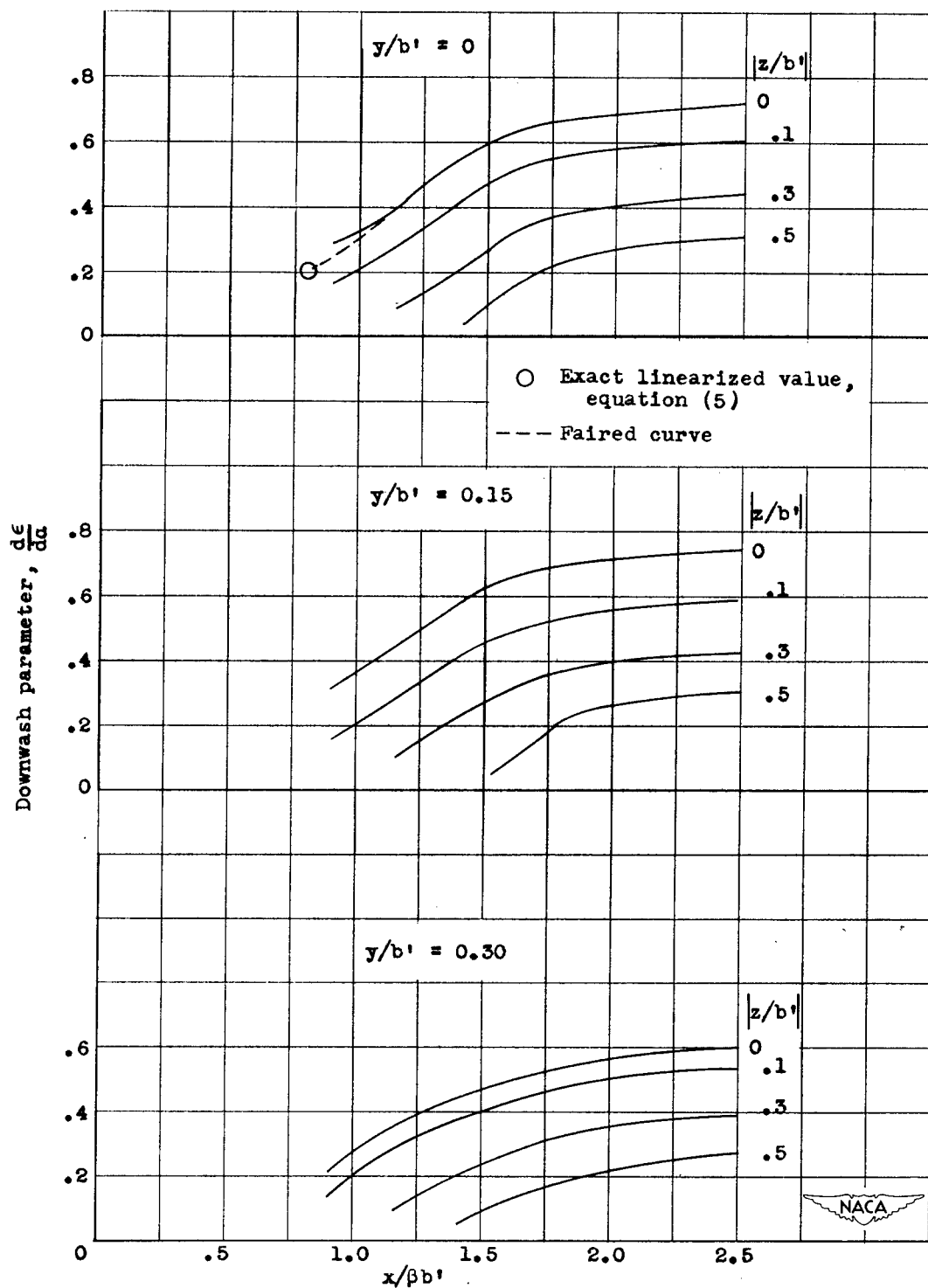
(b) Downwash near wing.

Figure 5. - Concluded. Charts showing plan form, load distribution, downwash in Trefftz plane, vortex-sheet displacement, and downwash near wing. Reduced aspect ratio, 2; root chord, $1.600 \beta b'$; lift coefficient, $3.25 \alpha/\beta$; midspan circulation, $2.273 \alpha U b'$.



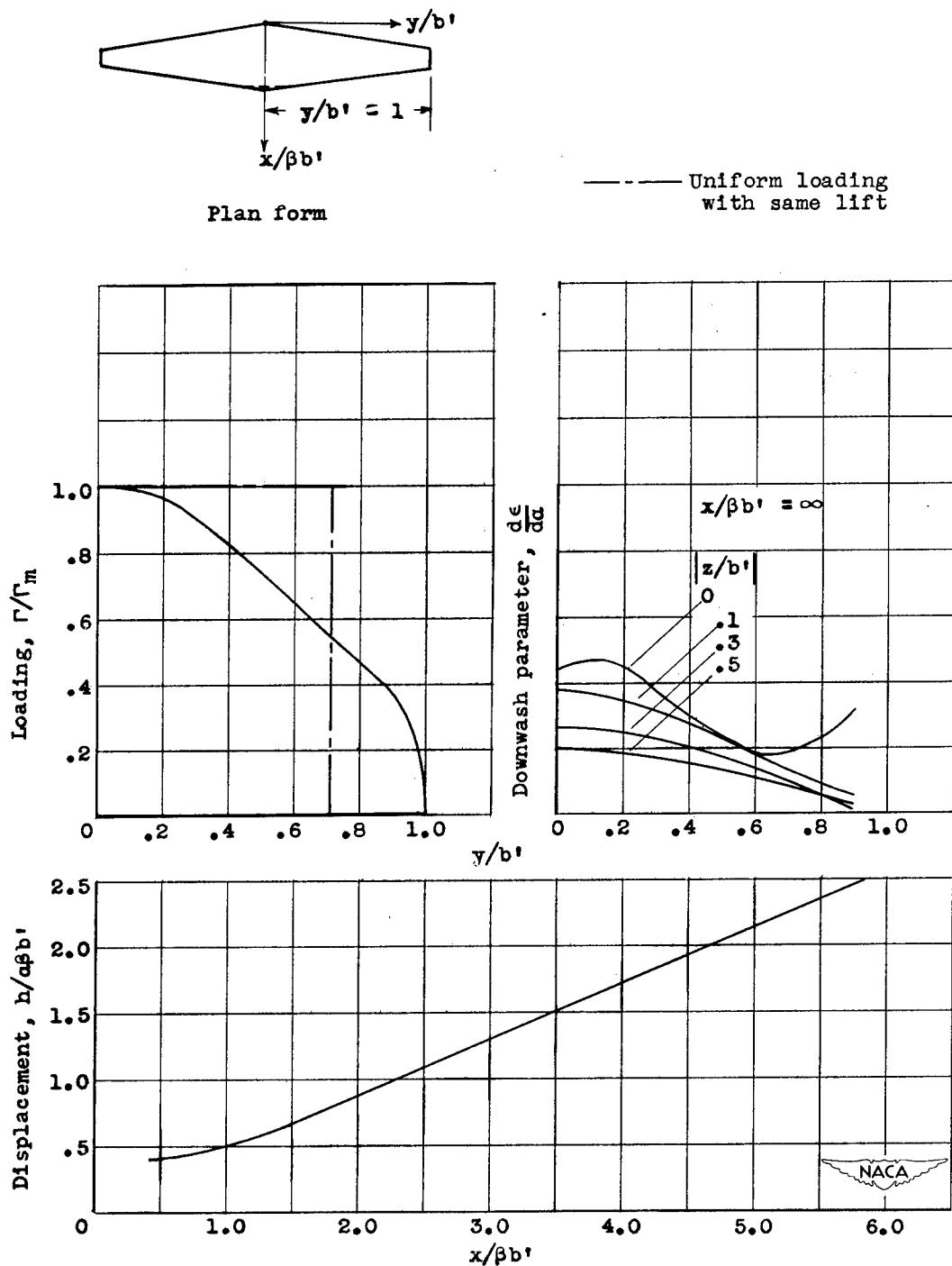
(a) Plan form, load distribution, downwash in Trefftz plane, and vortex-sheet displacement.

Figure 6. - Charts showing plan form, load distribution, downwash in Trefftz plane, vortex-sheet displacement, and downwash near wing. Reduced aspect ratio, 4; root chord, $0.800 \beta b'$; lift coefficient, $3.77 a/\beta$; midspan circulation, $1.301 aUb'$.



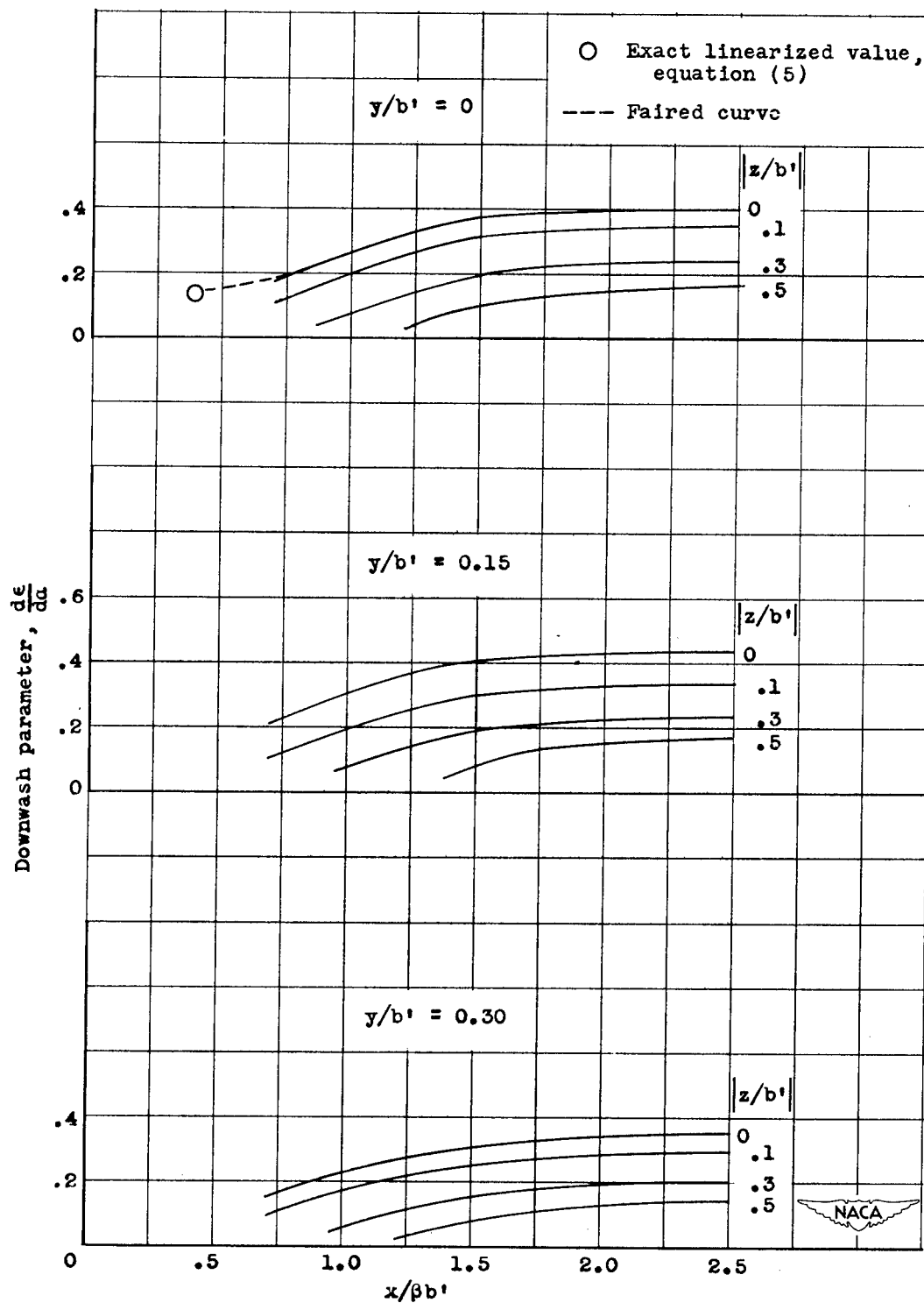
(b) Downwash near wing.

Figure 6. - Concluded. Charts showing plan form, load distribution, downwash in Trefftz plane, vortex-sheet displacement, and downwash near wing. Reduced aspect ratio, 4; root chord, $0.800 \beta b'$; lift coefficient, $3.77 \alpha/\beta$; midspan circulation, $1.301 \alpha U b'$.



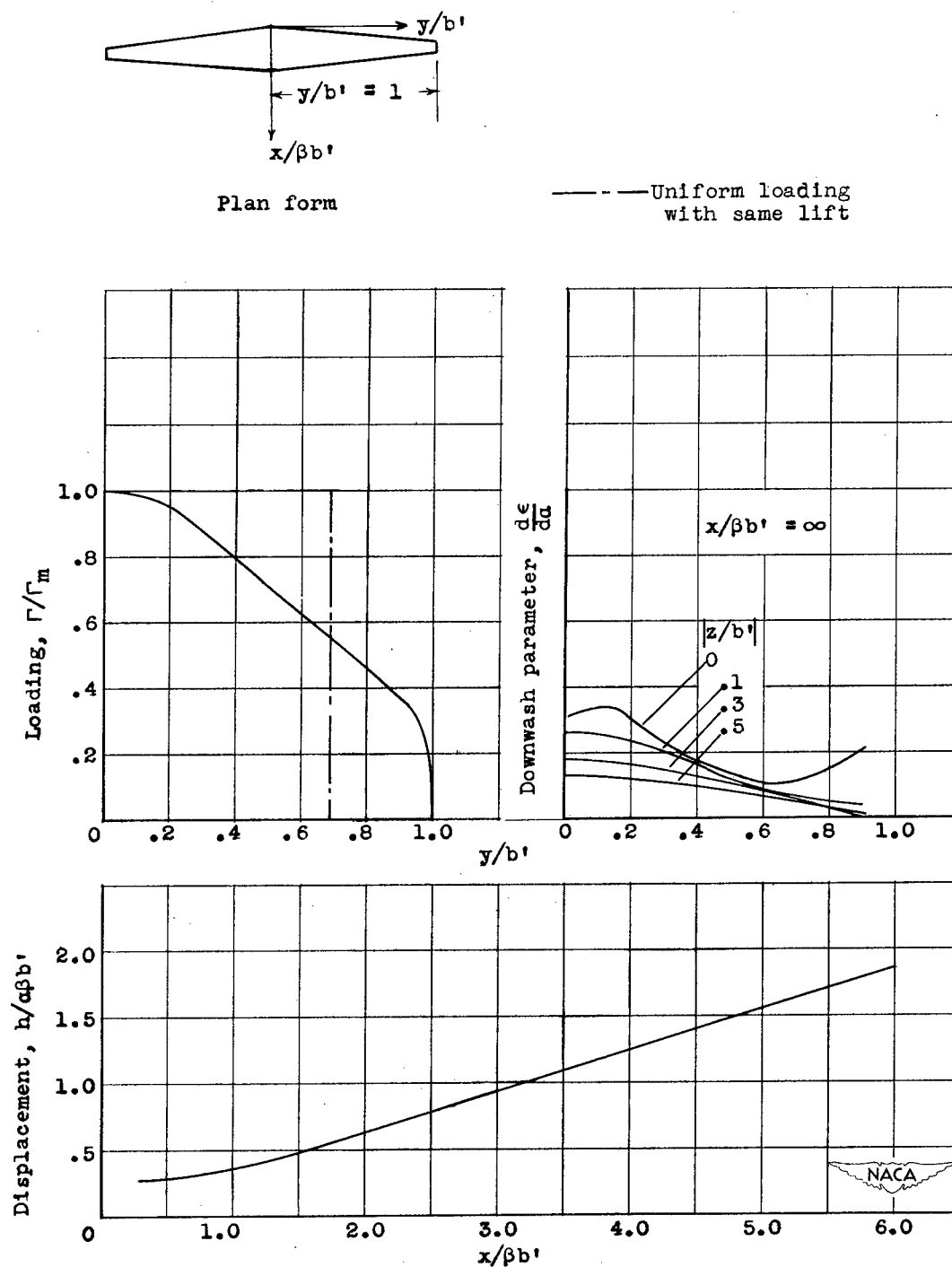
(a) Plan form, load distribution, downwash in Trefftz plane, and vortex-sheet displacement.

Figure 7. - Charts showing plan form, load distribution, downwash in Trefftz plane, vortex-sheet displacement, and downwash near wing. Reduced aspect ratio, 8; root chord, $0.400 \beta b'$; lift coefficient, $3.93 a/\beta$; midspan circulation, $0.704 aUb'$.



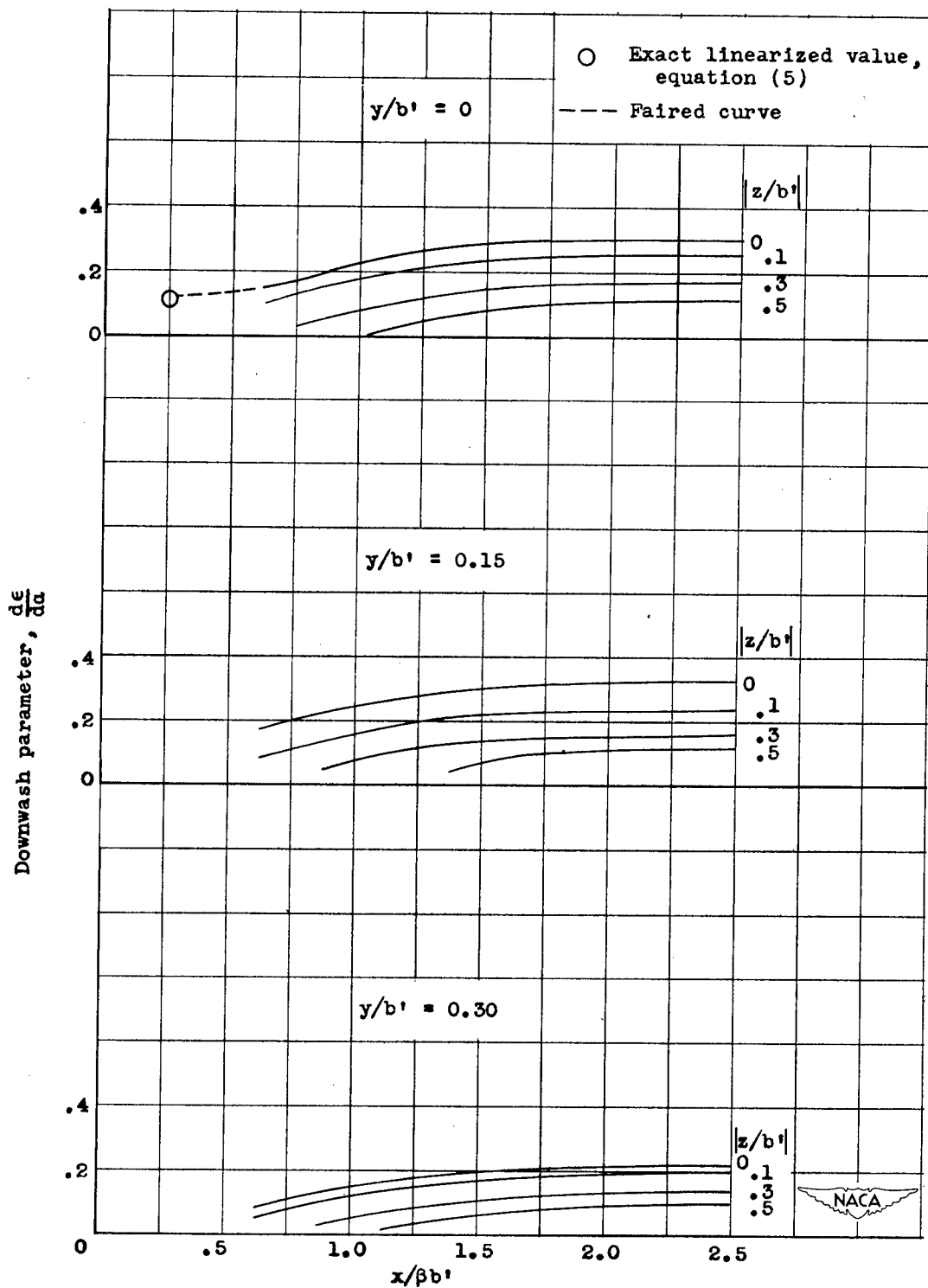
(b) Downwash near wing.

Figure 7. - Concluded. Charts showing plan form, load distribution, downwash in Trefftz plane, vortex-sheet displacement, and downwash near wing. Reduced aspect ratio, 8; root chord, $0.400 \beta b'$; lift coefficient, $3.93 a/\beta$; midspan circulation, $0.704 aUb'$.



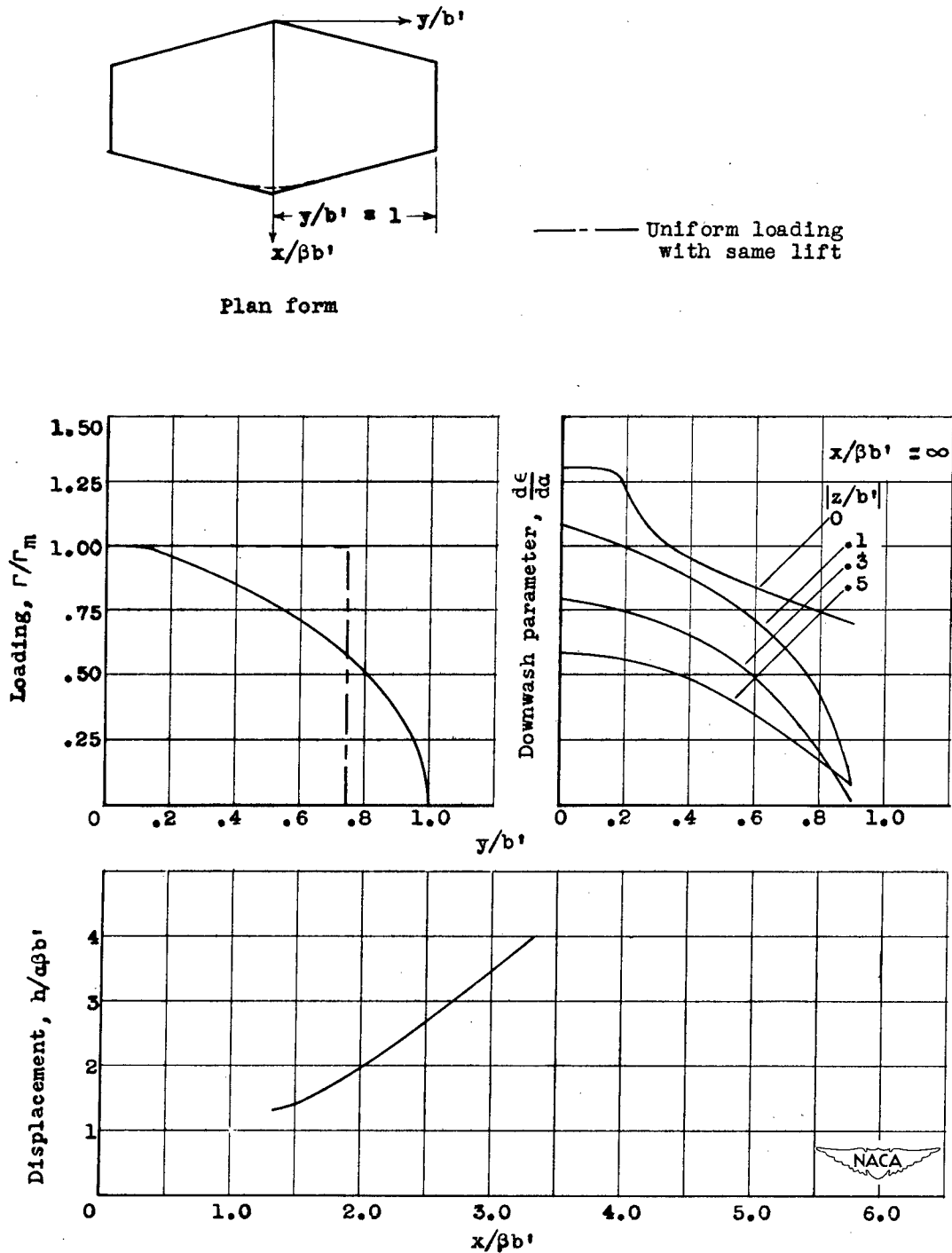
(a) Plan form, load distribution, downwash in Trefftz plane, and vortex-sheet displacement.

Figure 8. - Charts showing plan form, load distribution, downwash in Trefftz plane, vortex-sheet displacement, and downwash near wing. Reduced aspect ratio, 12; root chord, $0.267 \beta b'$; lift coefficient, $3.93 a/\beta$; midspan circulation, $0.483 aUb'$.



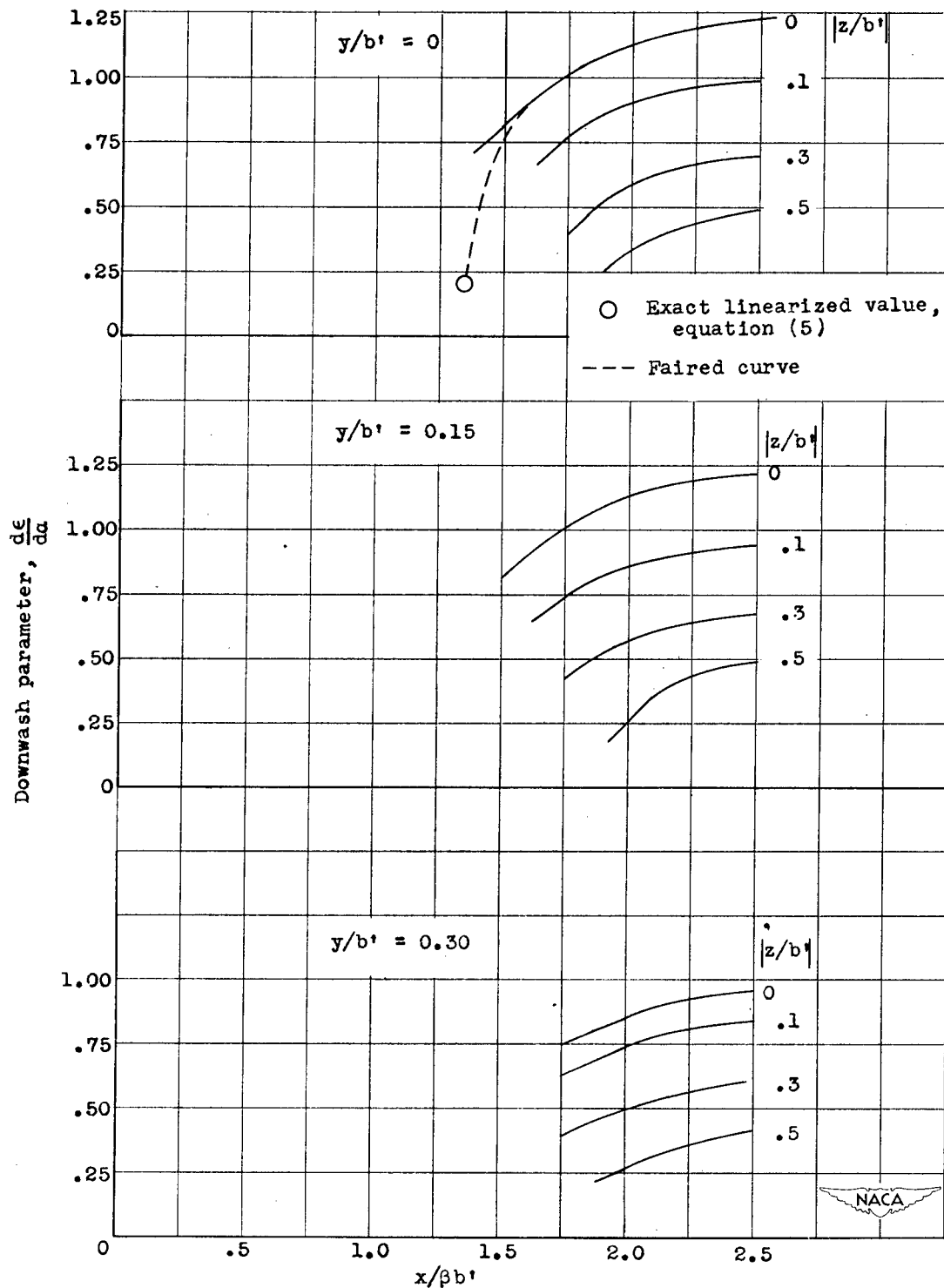
(b) Downwash near wing.

Figure 8. - Concluded. Charts showing plan form, load distribution, downwash in Trefftz plane, vortex-sheet displacement, and downwash near wing. Reduced aspect ratio, 12; root chord, $0.267 \beta b'$; lift coefficient, $3.93 \alpha/\beta$; midspan circulation, $0.483 \alpha U \beta b'$.



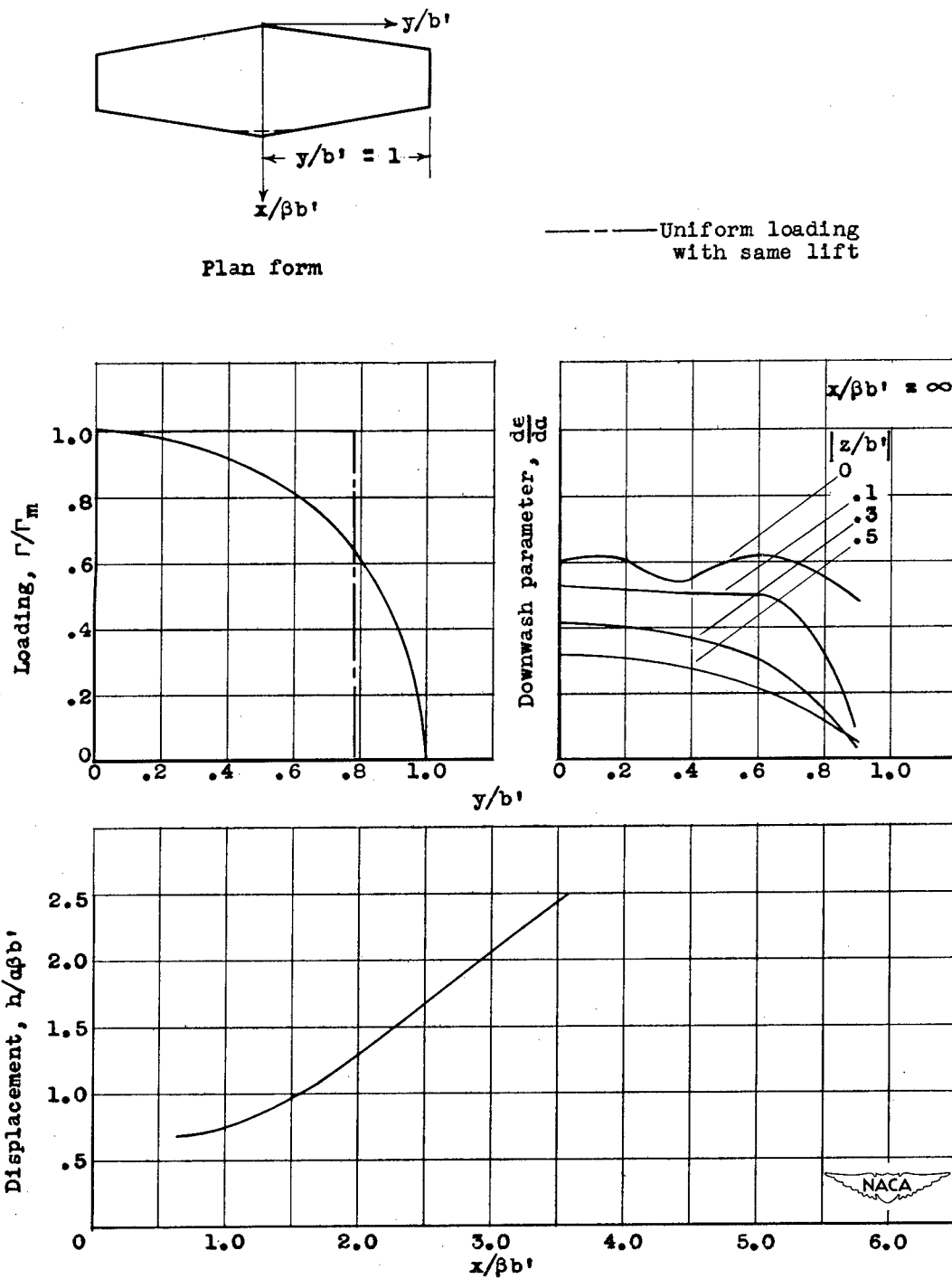
(a) Plan form, load distribution, downwash in Trefftz plane, and vortex-sheet displacement.

Figure 9. - Charts showing plan form, load distribution, downwash in Trefftz plane, vortex-sheet displacement, and downwash near wing. Reduced aspect ratio, 2; root chord, $1.333 \beta b'$; lift coefficient, $3.16 a/\beta$; midspan circulation, $2.161 aU_\infty b'$.



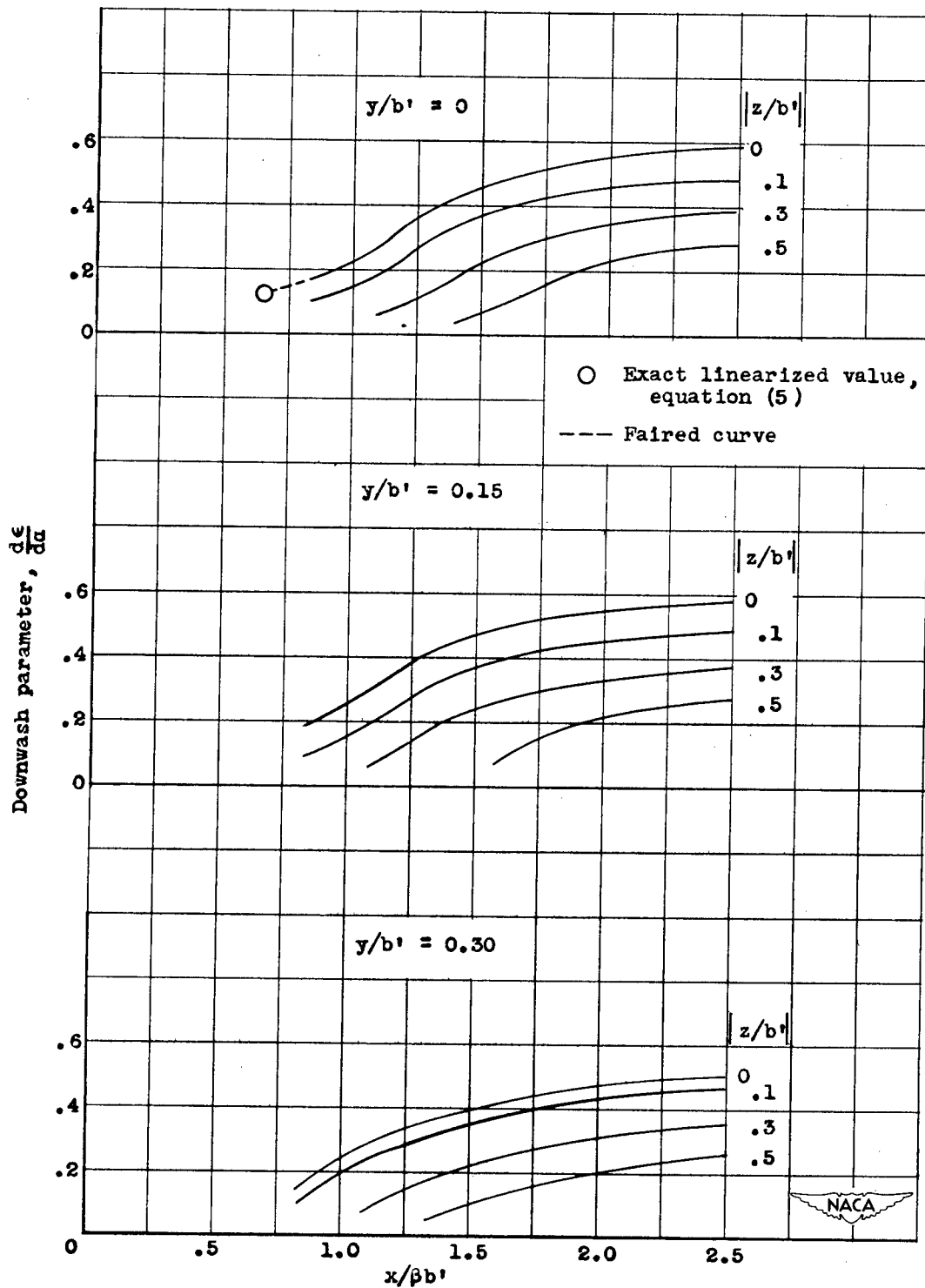
(b) Downwash near wing.

Figure 9. - Concluded. Charts showing plan form, load distribution, downwash in Trefftz plane, vortex-sheet displacement, and downwash near wing. Reduced aspect ratio, 2; root chord, $1.333 \beta b'$; lift coefficient, $3.16 \alpha/\beta$; midspan circulation, $2.161 \alpha U b'$.



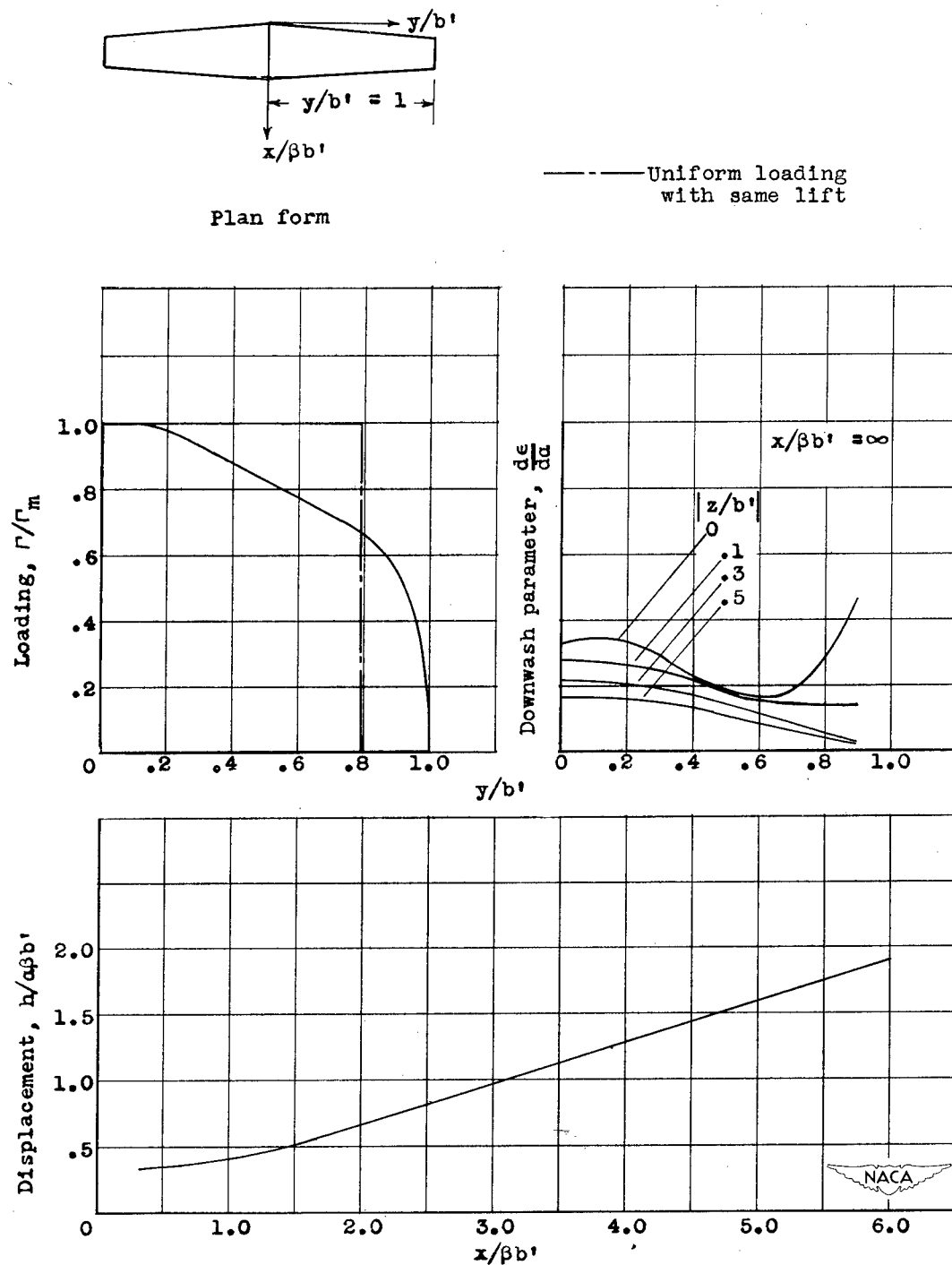
(a) Plan form, load distribution, downwash in Trefftz plane, and vortex-sheet displacement.

Figure 10. - Charts showing plan form, load distribution, downwash in Trefftz plane, vortex-sheet displacement, and downwash near wing. Reduced aspect ratio, 4; root chord, $0.667 \beta b'$; lift coefficient, $3.66 a/\beta$; midspan circulation, $1.178 aUb'$.



(b) Downwash near wing.

Figure 10. - Concluded. Charts showing plan form, load distribution, downwash in Trefftz plane, vortex-sheet displacement, and downwash near wing. Reduced aspect ratio, 4; root chord, $0.667 \beta b'$; lift coefficient, $3.66 \alpha/\beta$; midspan circulation, $1.178 \alpha U b'$.



(a) Plan form, load distribution, downwash in Trefftz plane, and vortex-sheet displacement.

Figure 11. - Charts showing plan form, load distribution, downwash in Trefftz plane, vortex-sheet displacement, and downwash near wing. Reduced aspect ratio, 8; root chord, $0.333 \beta b'$; lift coefficient, $3.90 a/\beta$; midspan circulation, $0.617 aUb'$.

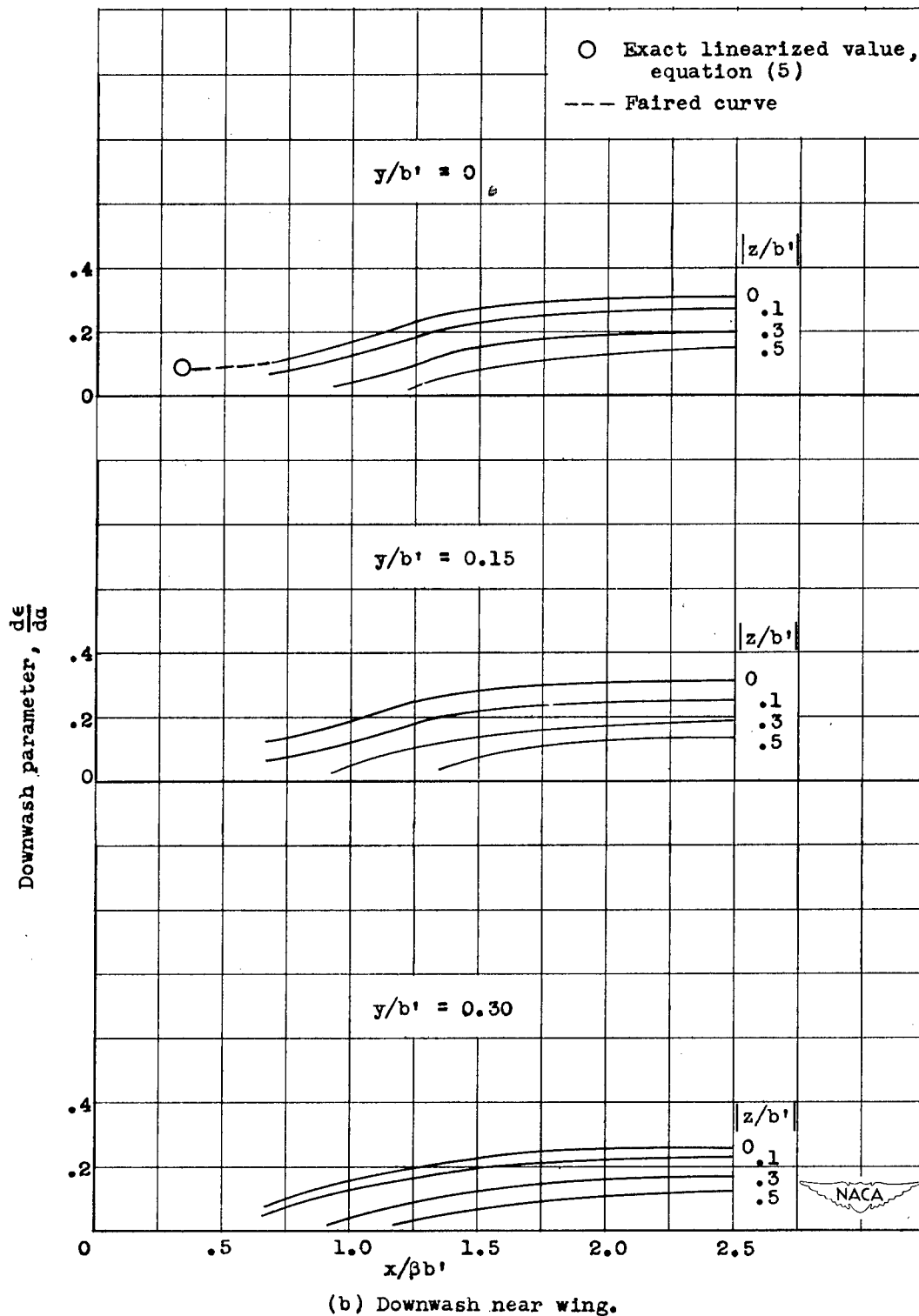
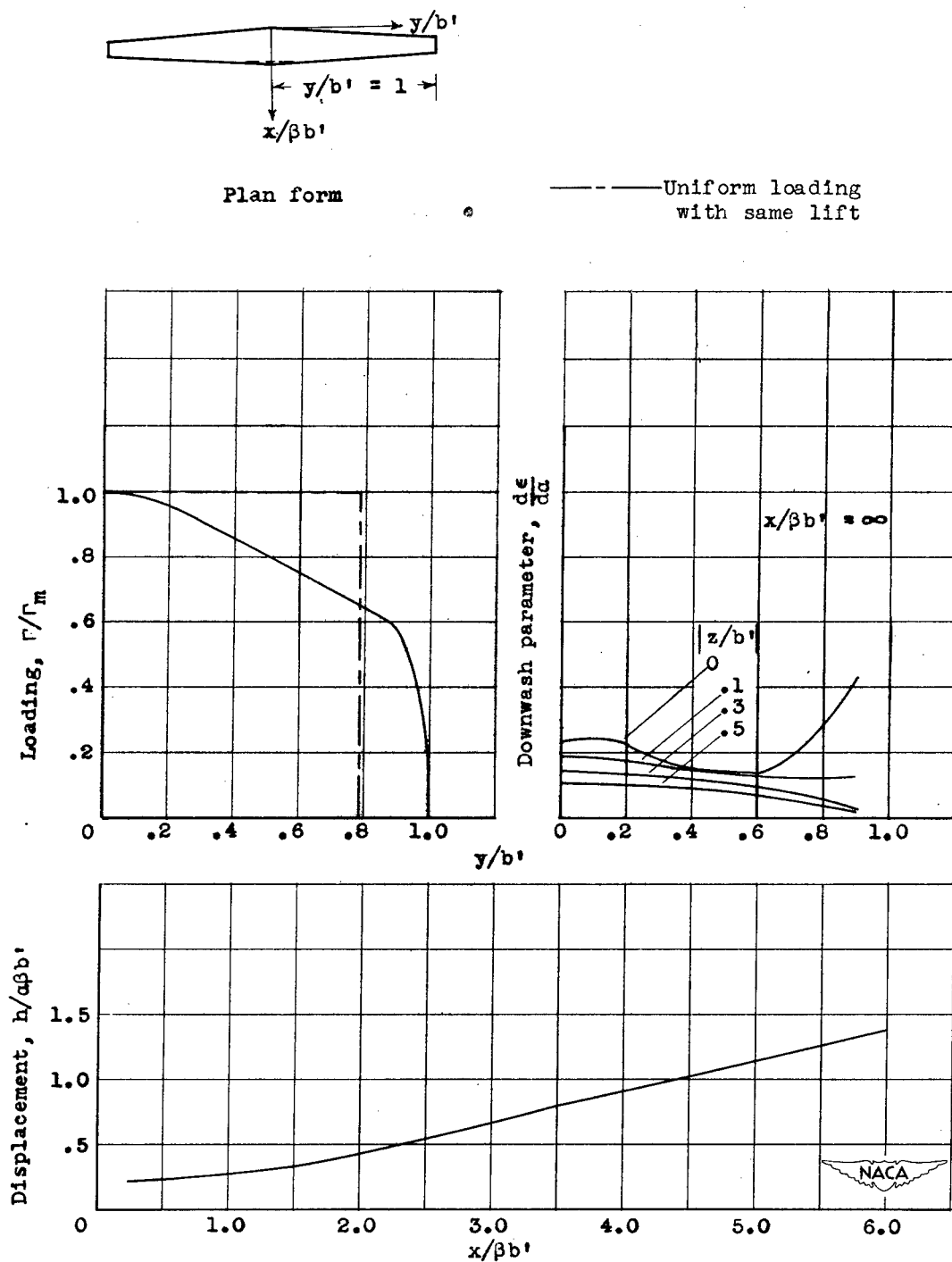
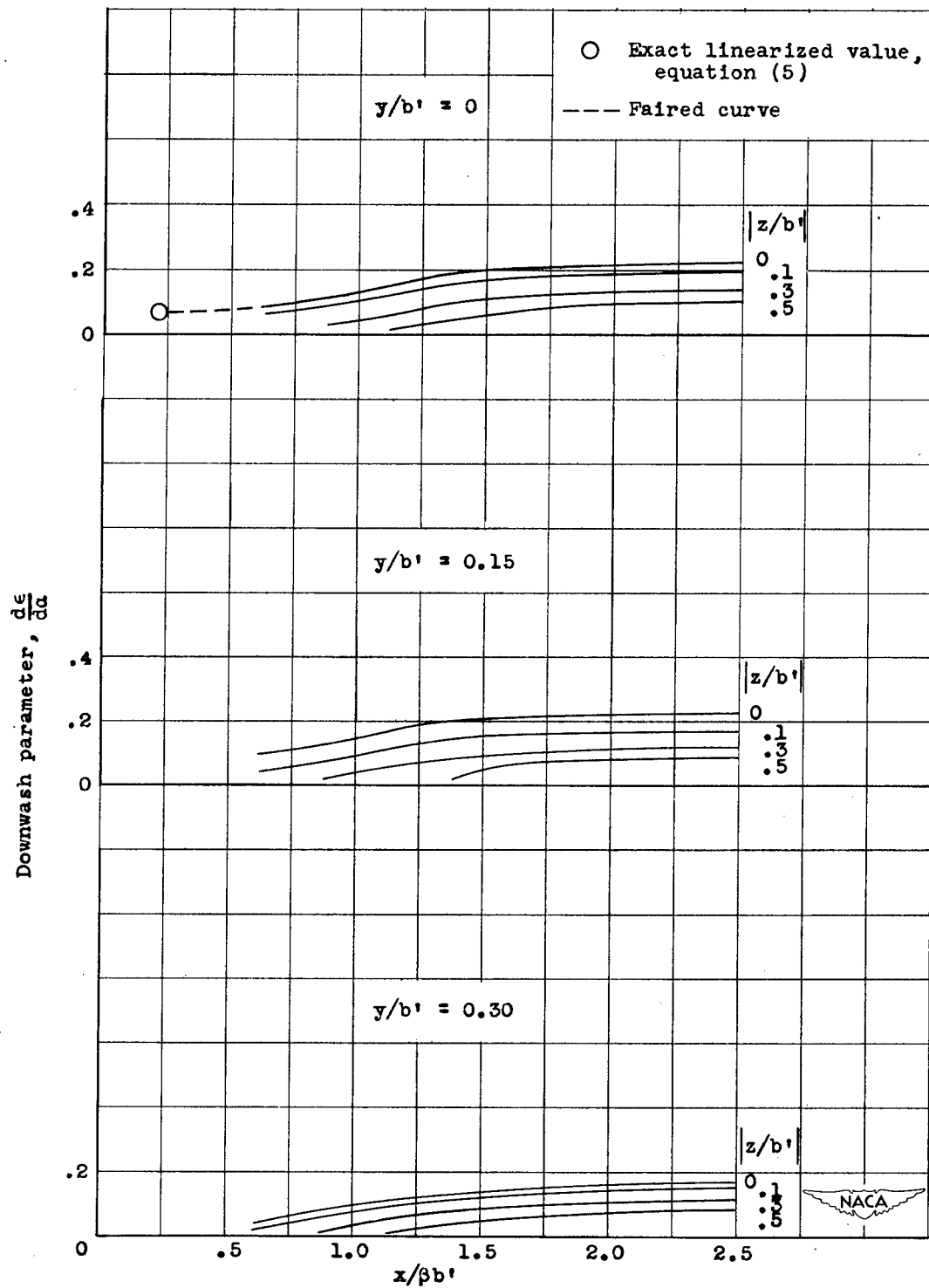


Figure 11. - Concluded. Charts showing plan form, load distribution, downwash in Trefftz plane, vortex-sheet displacement, and downwash near wing. Reduced aspect ratio, 8; root chord, $0.333 \beta b'$; lift coefficient, $3.90 \alpha/\beta$; midspan circulation, $0.617 \alpha U b'$.



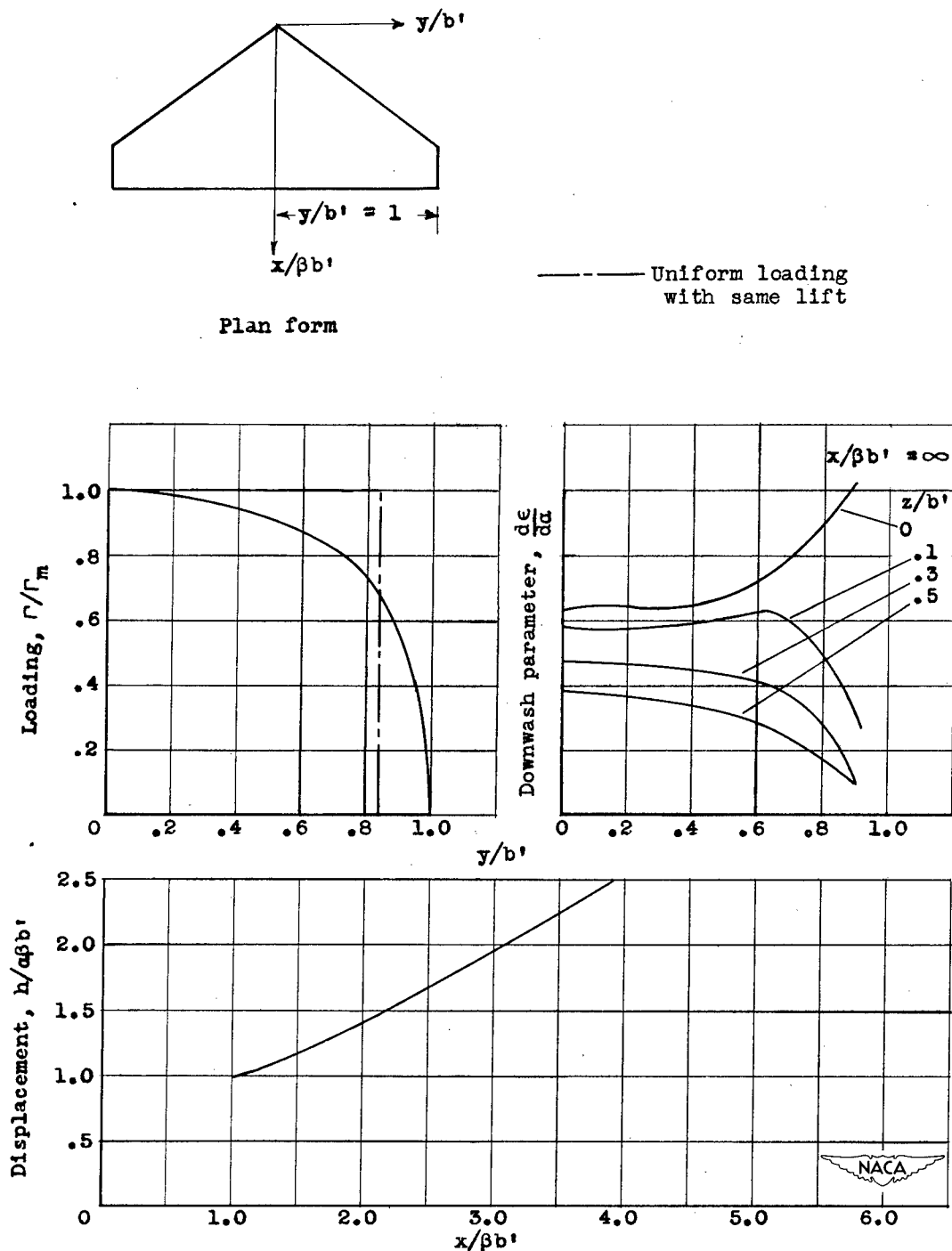
(a) Plan form, load distribution, downwash in Trefftz plane, and vortex-sheet displacement.

Figure 12. - Charts showing plan form, load distribution, downwash in Trefftz plane, vortex-sheet displacement, and downwash near wing. Reduced aspect ratio, 12; root chord, $0.222 \beta b'$; lift coefficient, $3.91 \alpha/\beta$; midspan circulation, $0.419 \alpha U b'$.



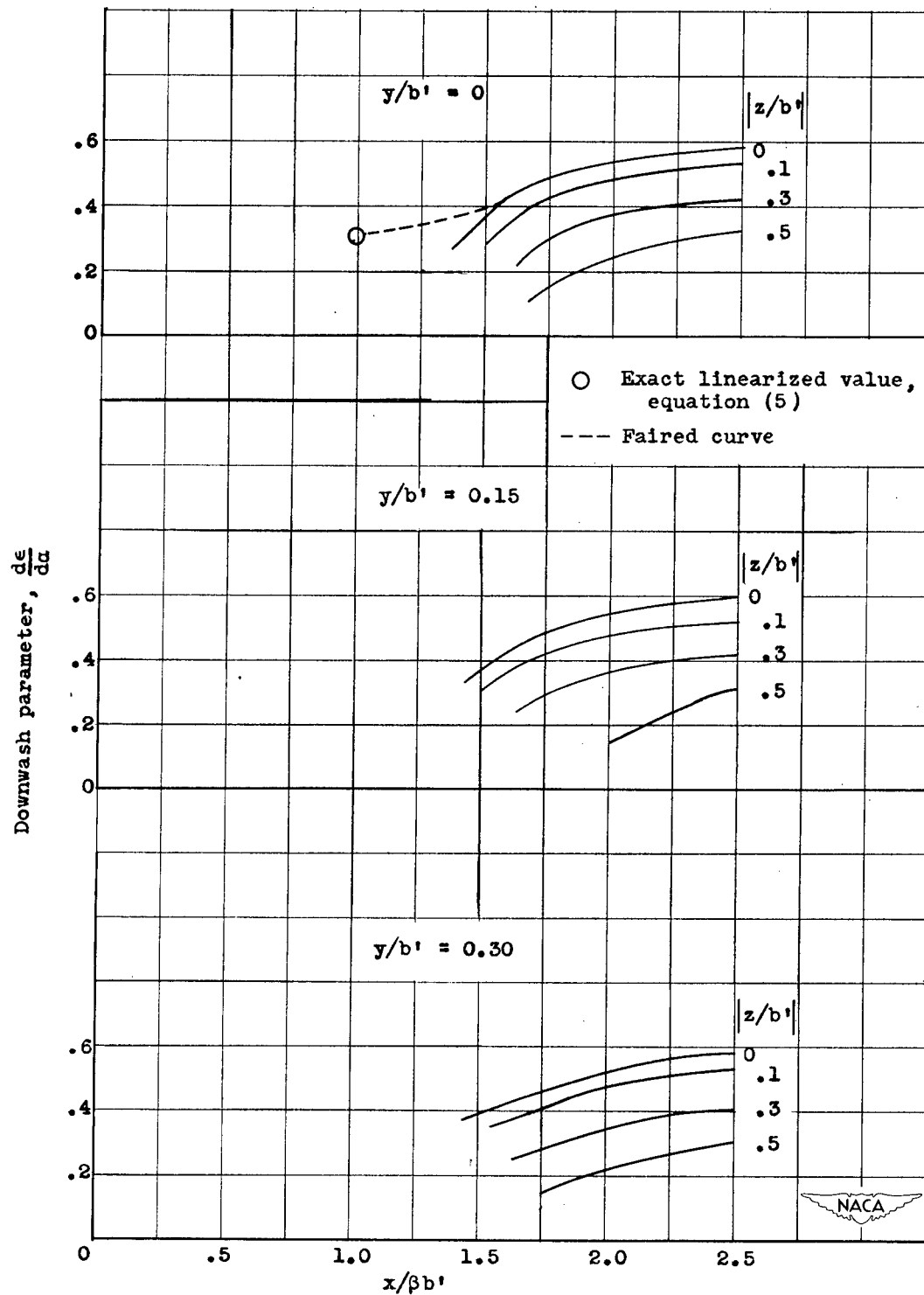
(b) Downwash near wing.

Figure 12. - Concluded. Charts showing plan form, load distribution, downwash in Trefftz plane, vortex-sheet displacement, and downwash near wing. Reduced aspect ratio, 12; root chord, $0.222 \beta b'$; lift coefficient, $3.91 a/\beta$; midspan circulation, $0.419 aUb'$.



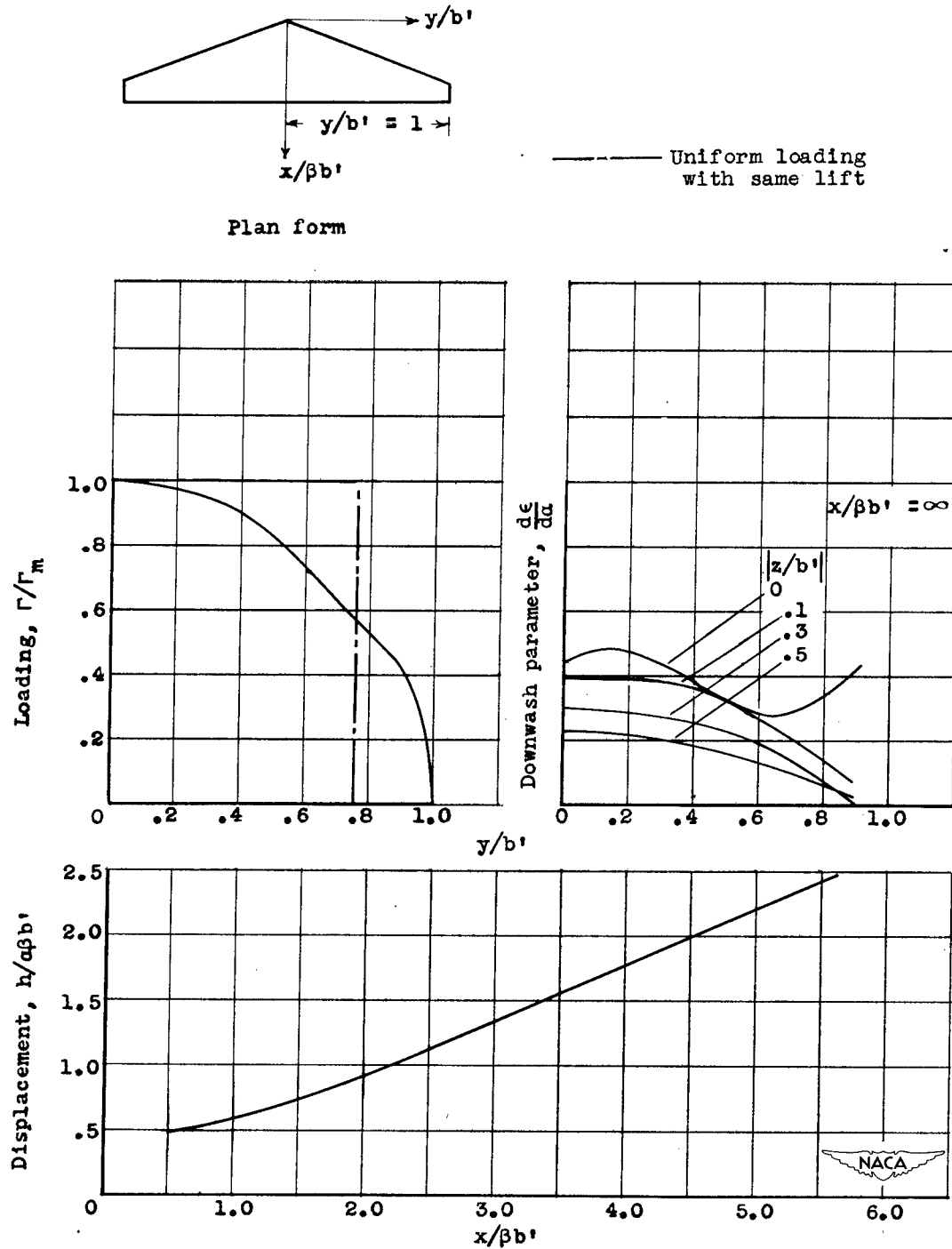
(a) Plan form, load distribution, downwash in Trefftz plane, and vortex-sheet displacement.

Figure 13. - Charts showing plan form, load distribution, downwash in Trefftz plane, vortex-sheet displacement, and downwash near wing. Reduced aspect ratio, 3.2; root chord, $1.000 \beta b'$; lift coefficient, $3.74 a/\beta$; midspan circulation, $1.391 aUb'$.



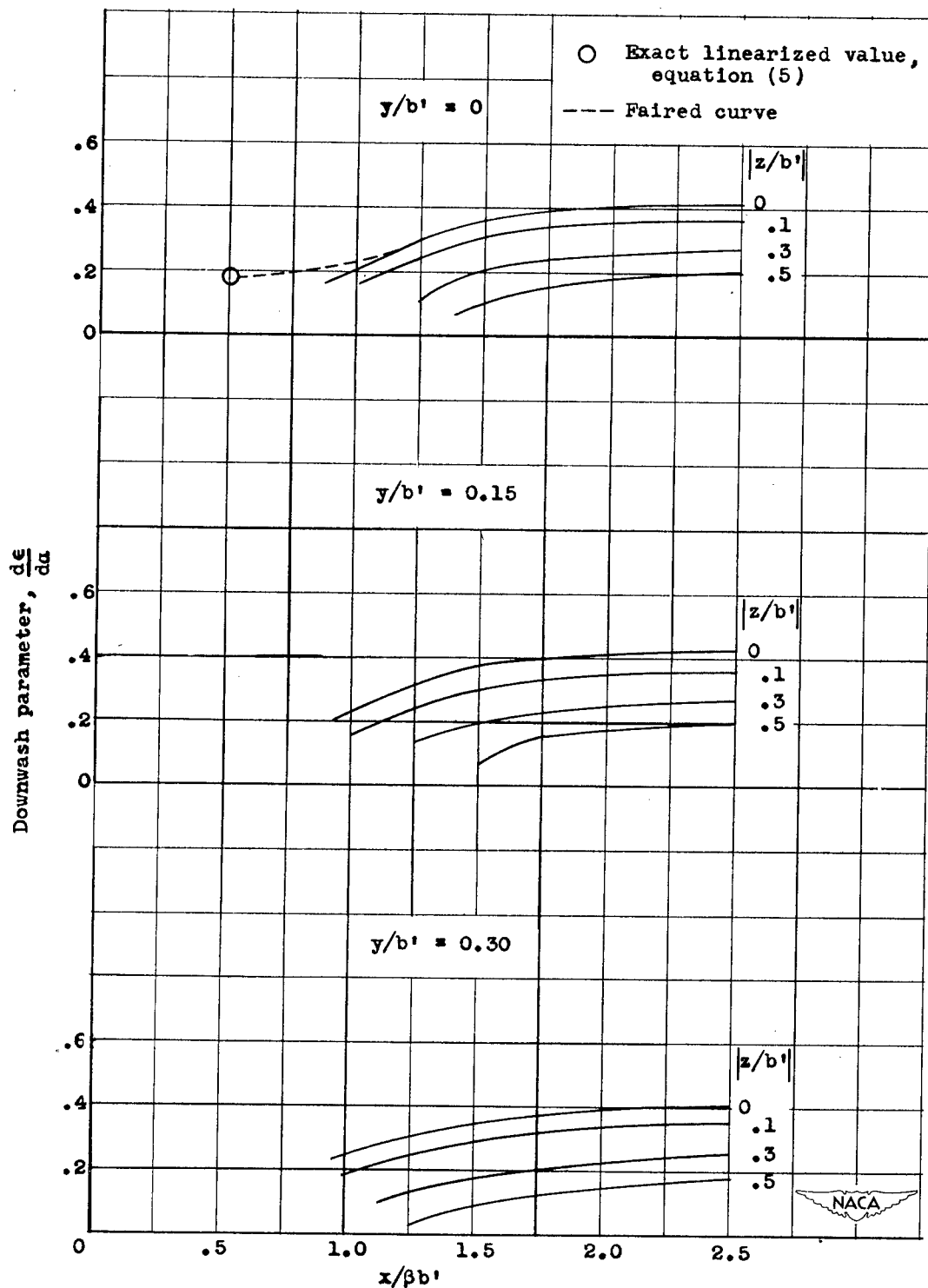
(b) Downwash near wing.

Figure 13. - Concluded. Charts showing plan form, load distribution, downwash in Trefftz plane, vortex-sheet displacement, and downwash near wing. Reduced aspect ratio, 3.2; root chord, $1.000 \beta b'$; lift coefficient, $3.74 a/\beta$; midspan circulation, $1.391 aUb'$.



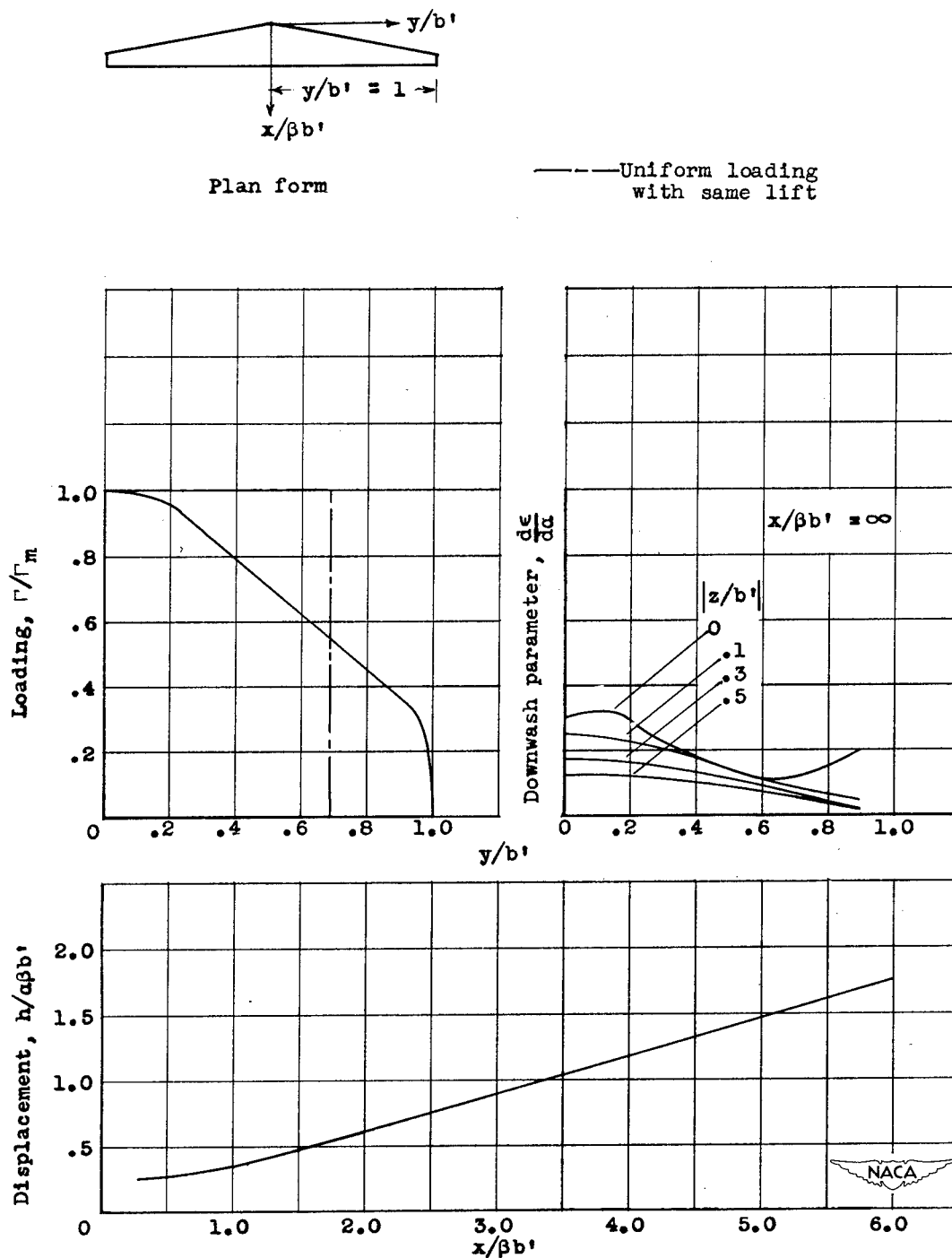
(a) Plan form, load distribution, downwash in Trefftz plane, and vortex-sheet displacement.

Figure 14. - Charts showing plan form, load distribution, downwash in Trefftz plane, vortex-sheet displacement, and downwash near wing. Reduced aspect ratio, 6.4; root chord, $0.500 \beta b'$; lift coefficient, $3.95 a/\beta$; midspan circulation, $0.815 aUb'$.



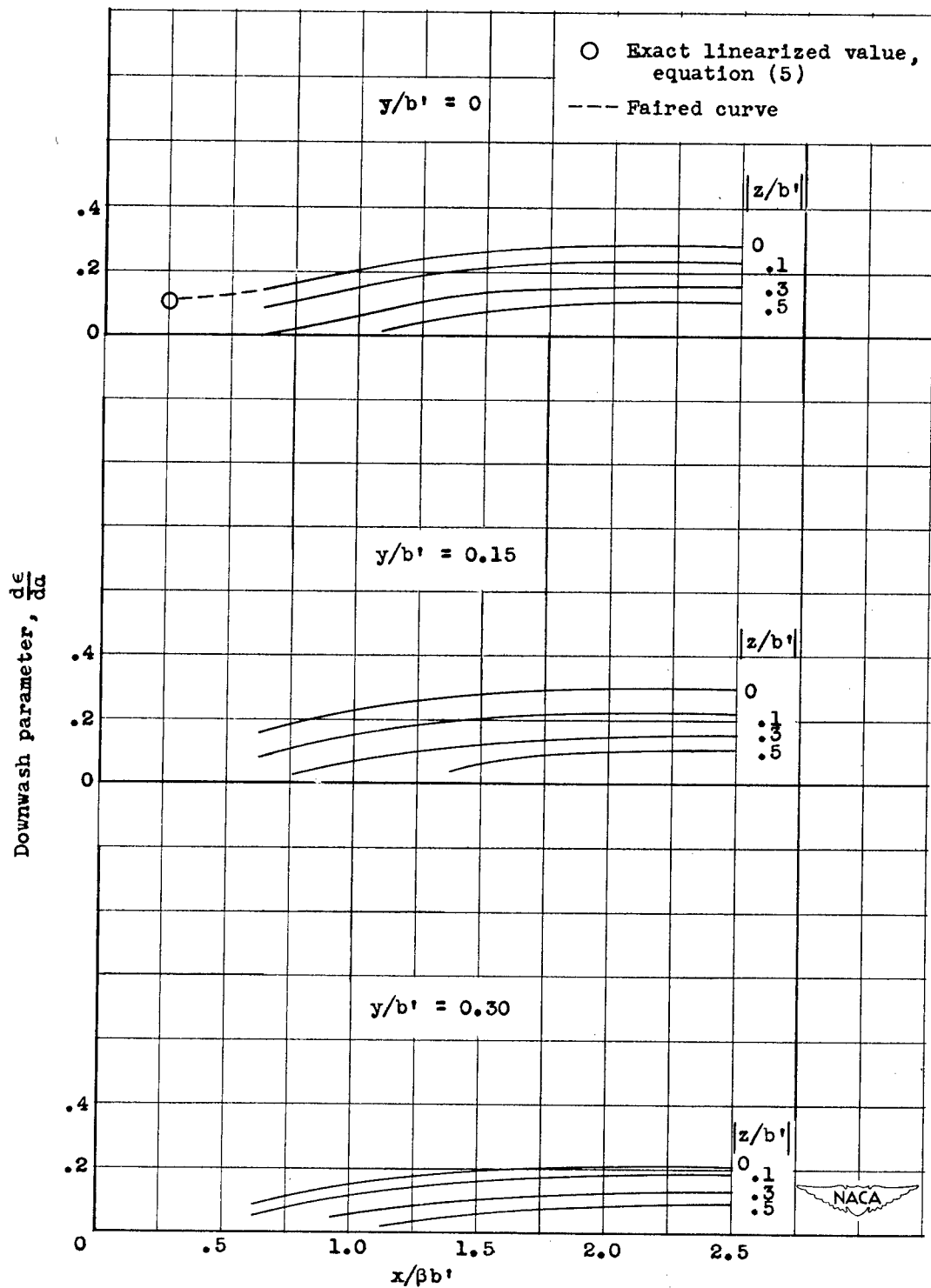
(b) Downwash near wing.

Figure 14. - Concluded. Charts showing plan form, load distribution, downwash in Trefftz plane, vortex-sheet displacement, and downwash near wing. Reduced aspect ratio, 6.4; root chord, $0.500 \beta b'$; lift coefficient, $3.95 a/\beta$; midspan circulation, $0.815 aUb'$.



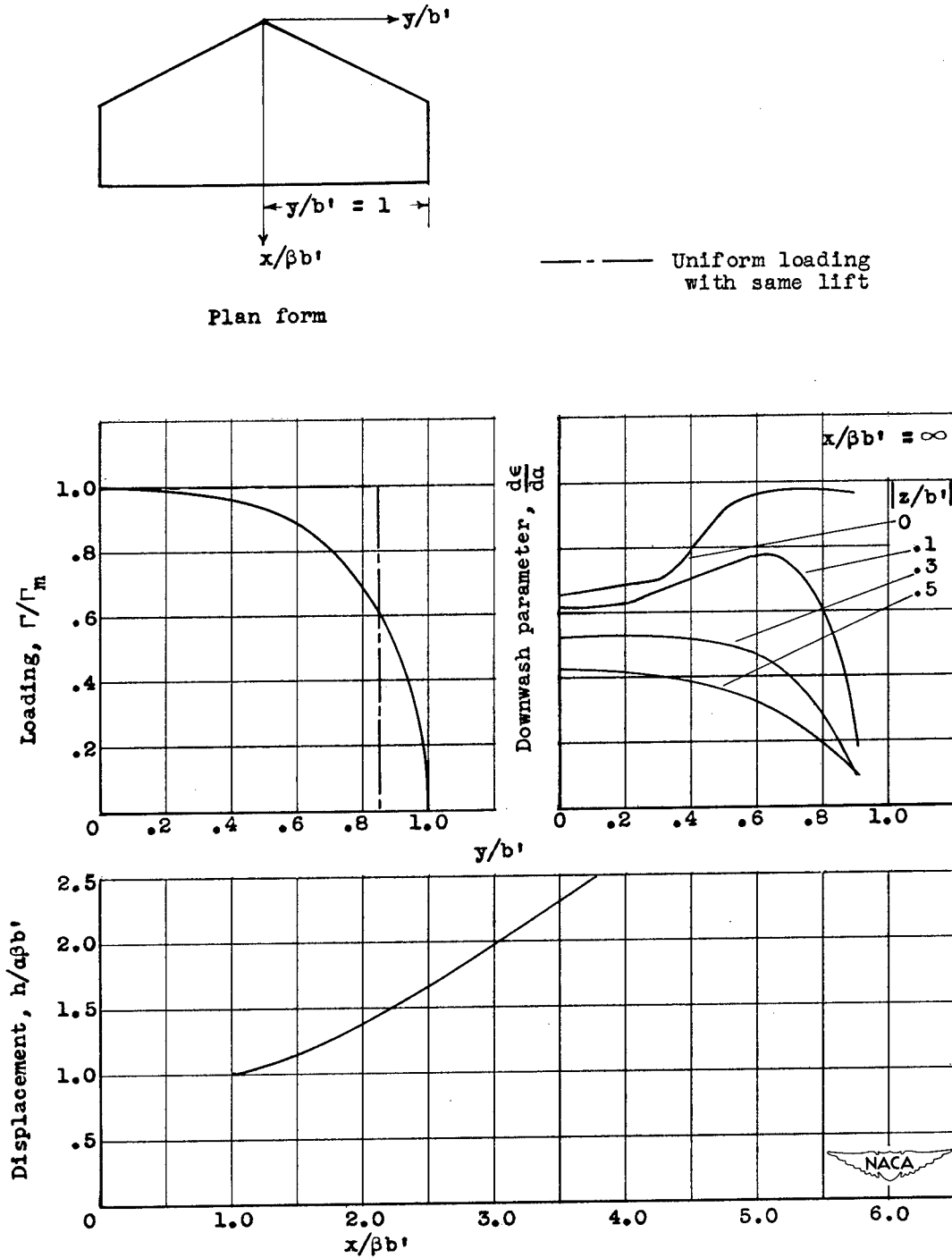
(a) Plan form, load distribution, downwash in Trefftz plane, and vortex-sheet displacement.

Figure 15. - Charts showing plan form, load distribution, downwash in Trefftz plane, vortex-sheet displacement, and downwash near wing. Reduced aspect ratio, 12.8; root chord, $0.250 \beta b'$; lift coefficient, $3.96 \alpha/\beta$; midspan circulation, $0.448 \alpha U \beta b'$.



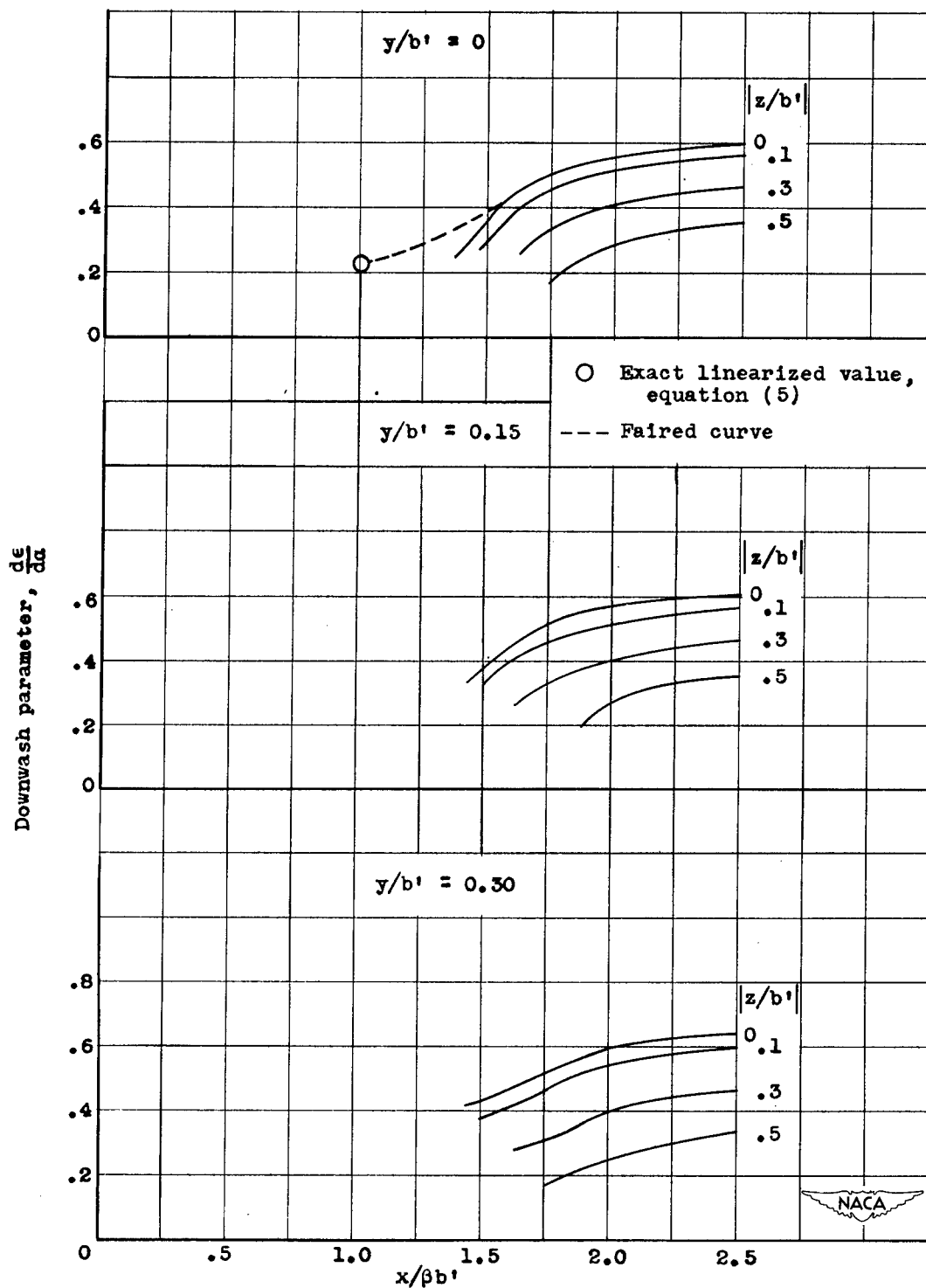
(b) Downwash near wing.

Figure 15. - Concluded. Charts showing plan form, load distribution, downwash in Trefftz plane, vortex-sheet displacement, and downwash near wing. Reduced aspect ratio, 12.8; root chord, $0.250 \beta b'$; lift coefficient, $3.96 \alpha/\beta$; midspan circulation, $0.448 \alpha U b'$.



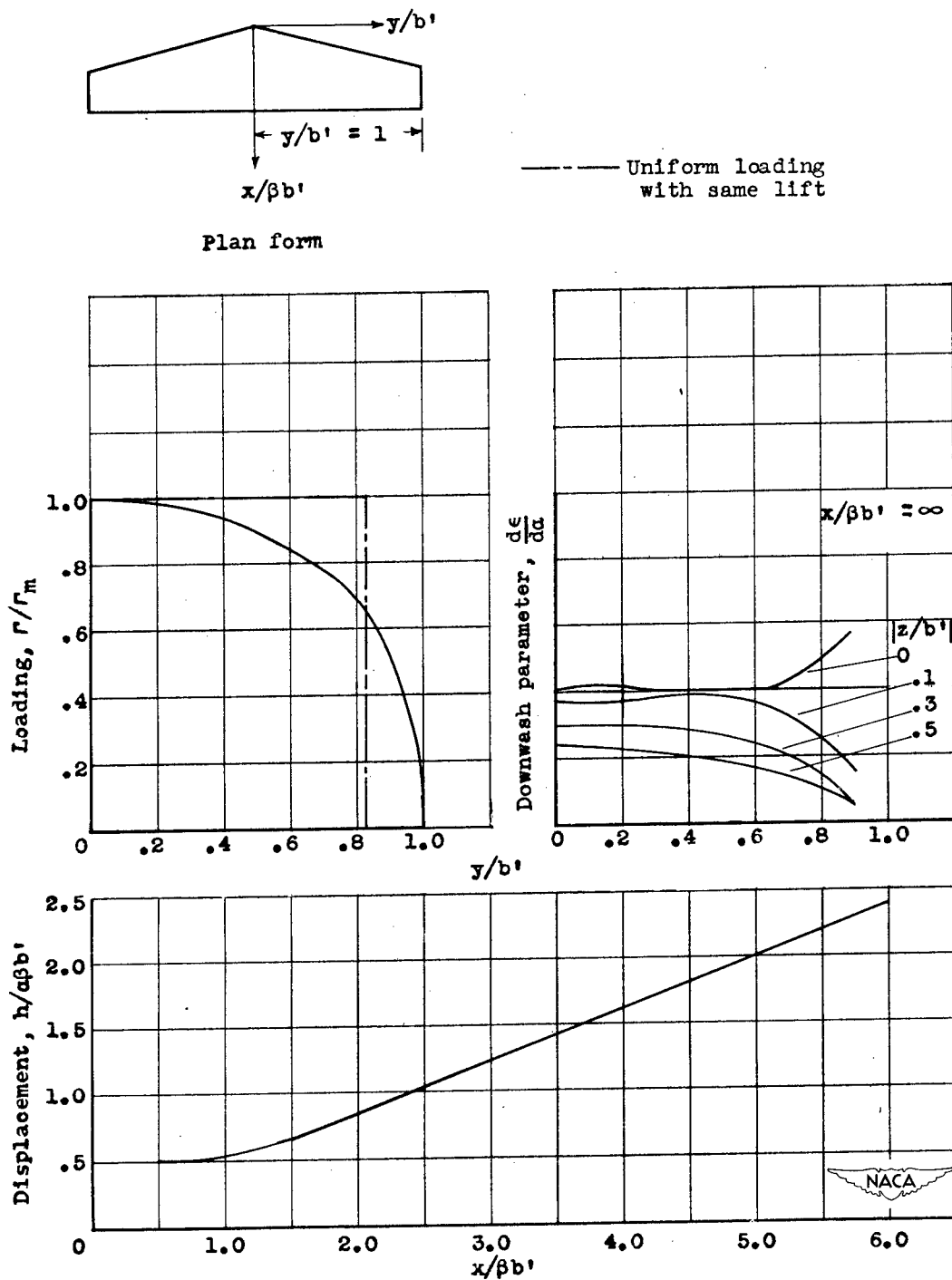
(a) Plan form, load distribution, downwash in Trefftz plane, and vortex-sheet displacement.

Figure 16. - Charts showing plan form, load distribution, downwash in Trefftz plane, vortex-sheet displacement, and downwash near wing. Reduced aspect ratio, 2.7; root chord, 1.000 $\beta b'$; lift coefficient, 3.46 a/β ; midspan circulation, 1.540 aUb' .



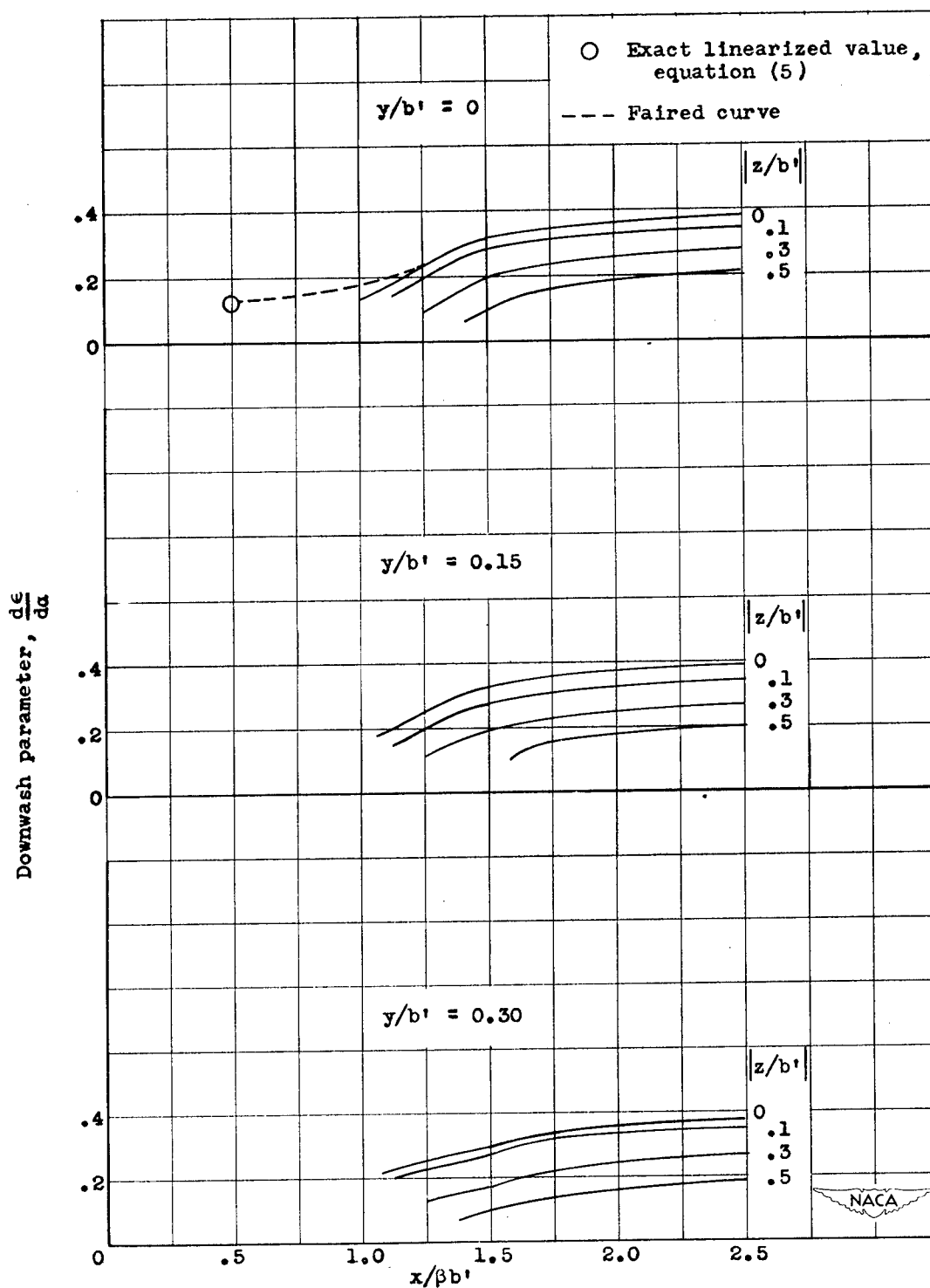
(b) Downwash near wing.

Figure 16. - Concluded. Charts showing plan form, load distribution, downwash in Trefftz plane, vortex-sheet displacement, and downwash near wing. Reduced aspect ratio, 2.7; root chord, $1.000 \beta b'$; lift coefficient, $3.46 a/\beta$; midspan circulation, $1.540 aUb'$.



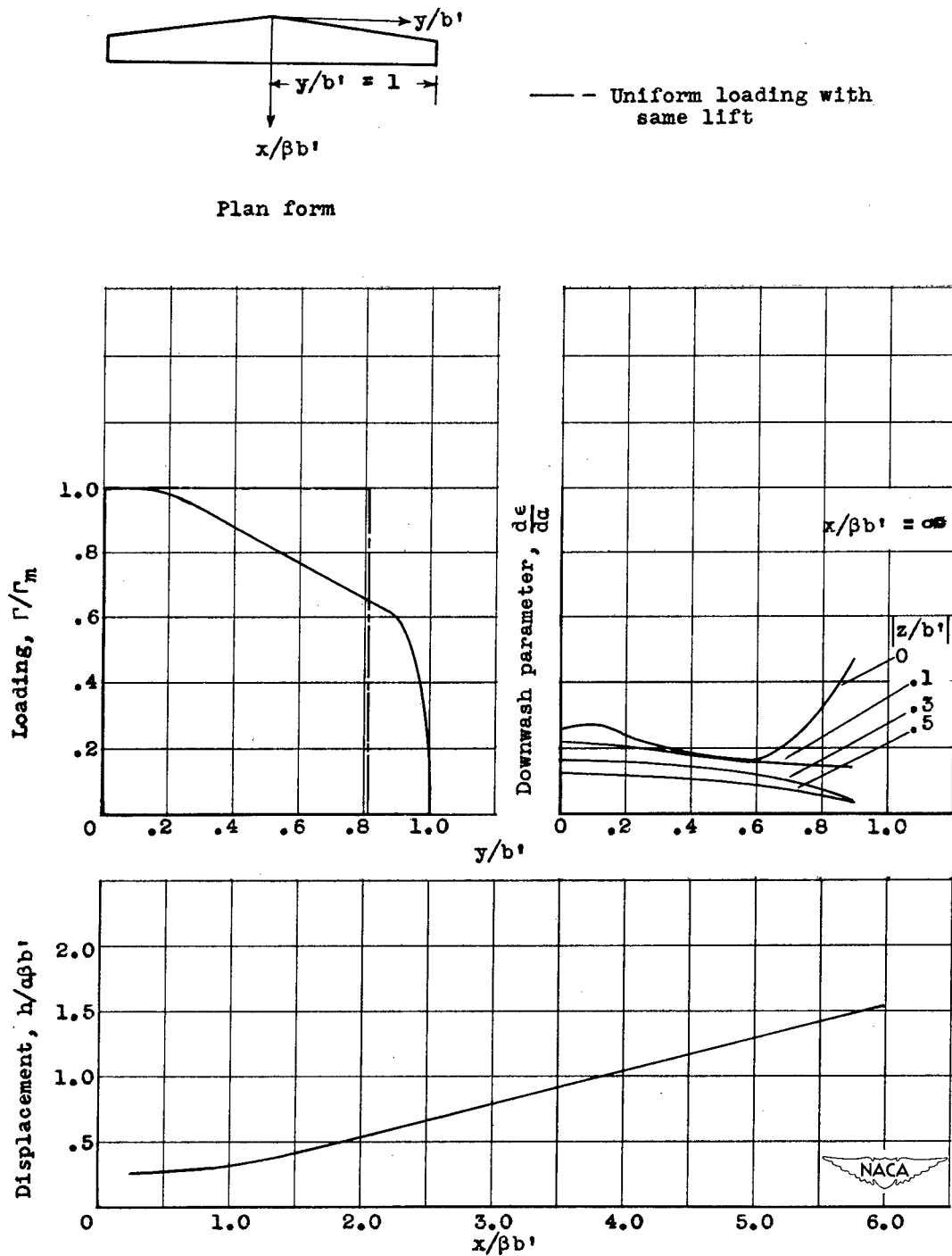
(a) Plan form, load distribution, downwash in Trefftz plane, and vortex-sheet displacement.

Figure 17. - Charts showing plan form, load distribution, downwash in Trefftz plane, vortex-sheet displacement, and downwash near wing. Reduced aspect ratio, 5.3; root chord, $0.500 \beta b'$; lift coefficient, $3.80 a/\beta$; midspan circulation, $0.867 aUb'$.



(b) Downwash near wing.

Figure 17. - Concluded. Charts showing plan form, load distribution, downwash in Trefftz plane, vortex-sheet displacement, and downwash near wing. Reduced aspect ratio, 5.3; root chord, $0.500 \beta b'$; lift coefficient, $3.80 \alpha/\beta$; midspan circulation, $0.867 \alpha U b'$.



(a) Plan form, load distribution, downwash in Trefftz plane, and vortex-sheet displacement.

Figure 18. - Charts showing plan form, load distribution, downwash in Trefftz plane, vortex-sheet displacement, and downwash near wing. Reduced aspect ratio, 10.7; root chord, $0.250 \beta b'$; lift coefficient, $3.91 a/\beta$; midspan circulation, $0.464 aUb'$.

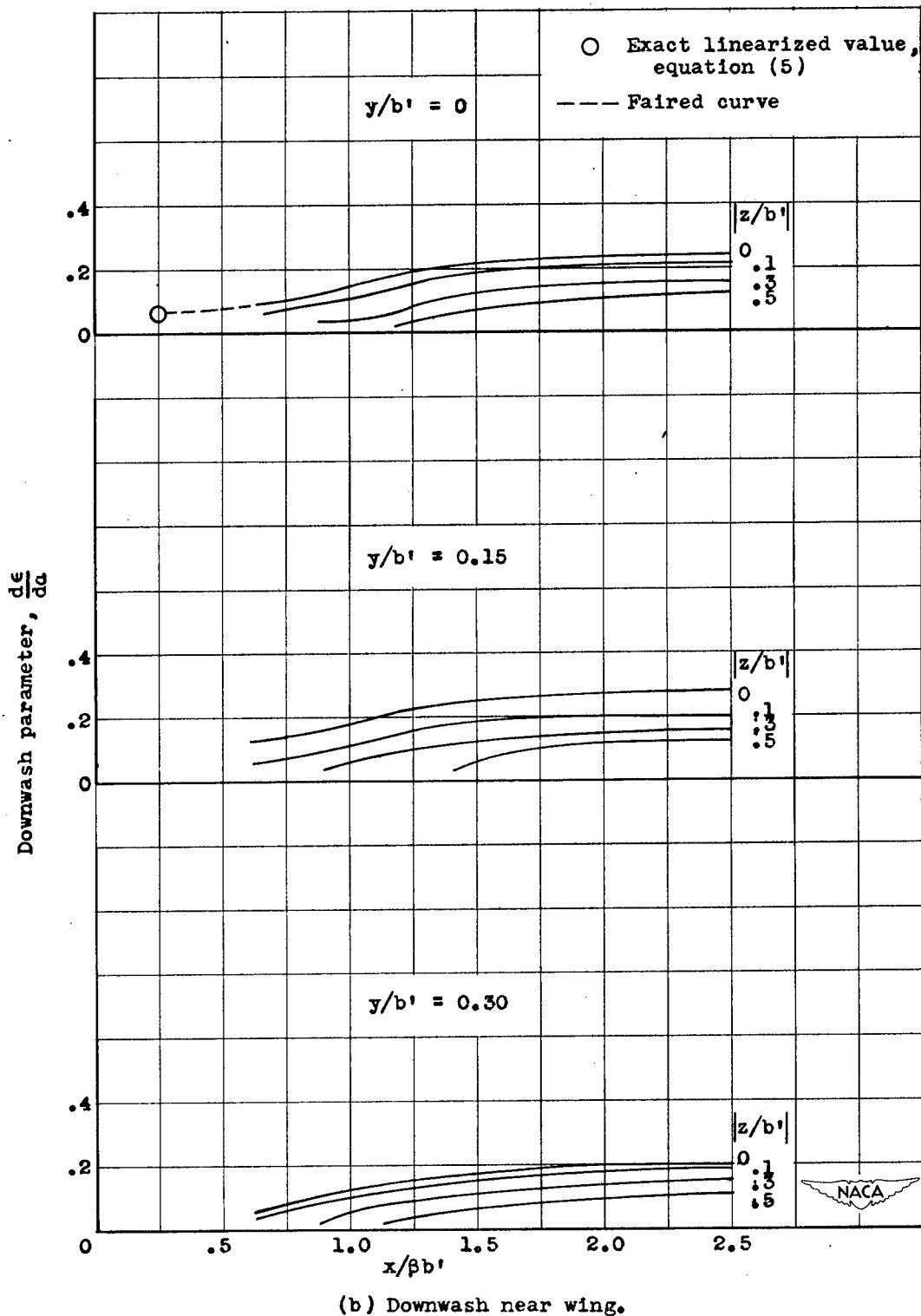
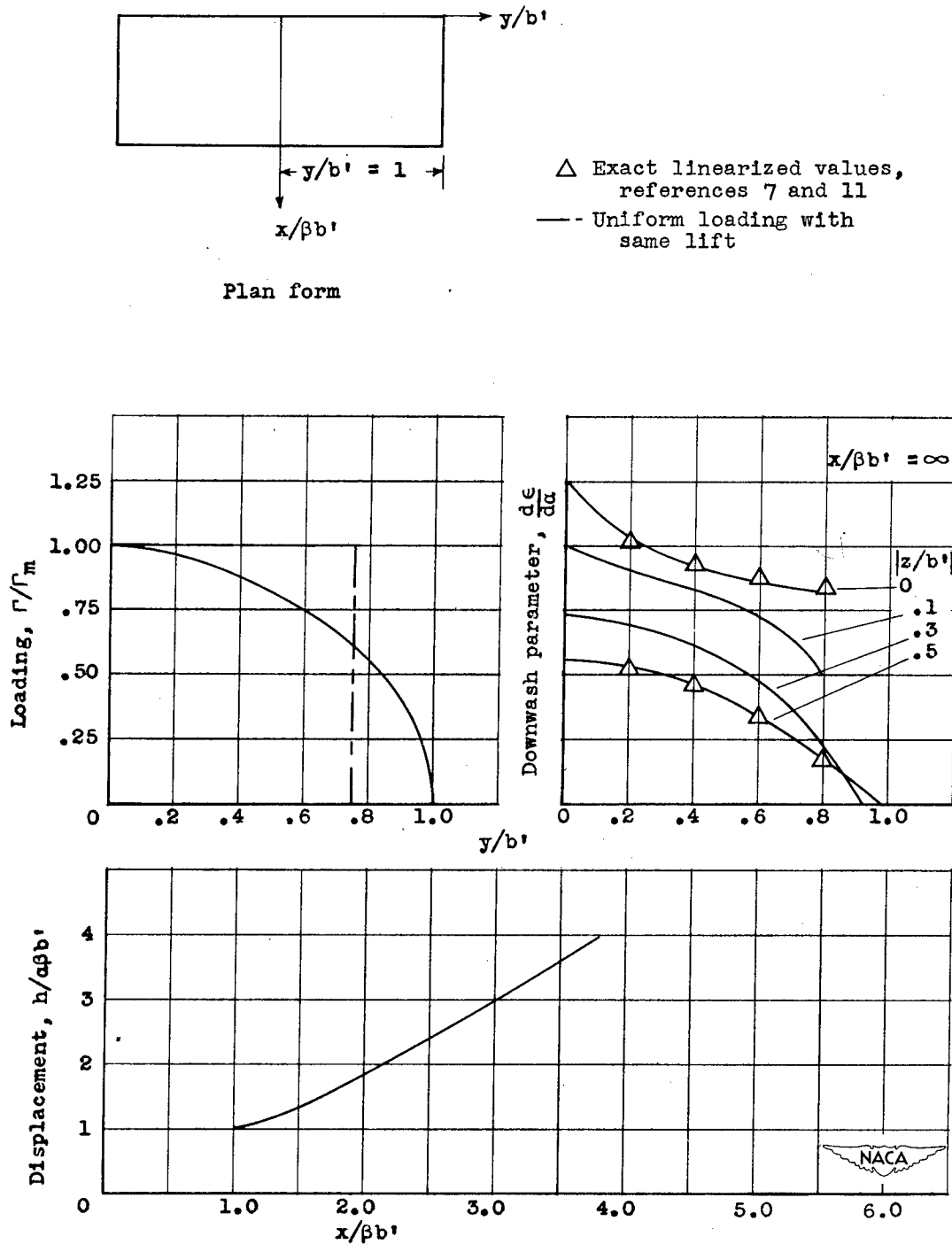
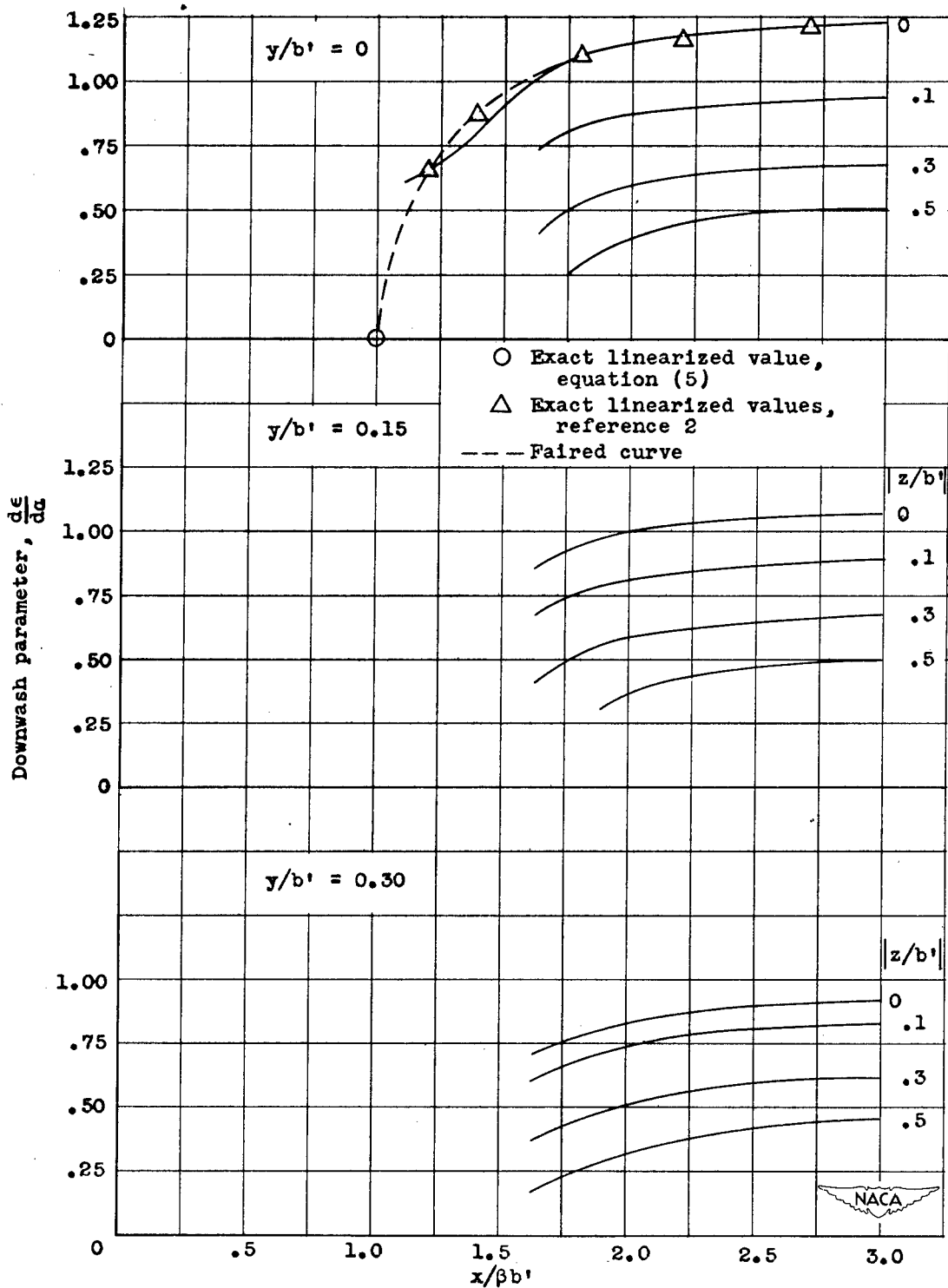


Figure 18. - Concluded. Charts showing plan form, load distribution, downwash in Trefftz plane, vortex-sheet displacement, and downwash near wing. Reduced aspect ratio, 10.7; root chord, $0.250 \beta b'$; lift coefficient, 3.91 a/β ; midspan circulation, $0.464 aUb'$.



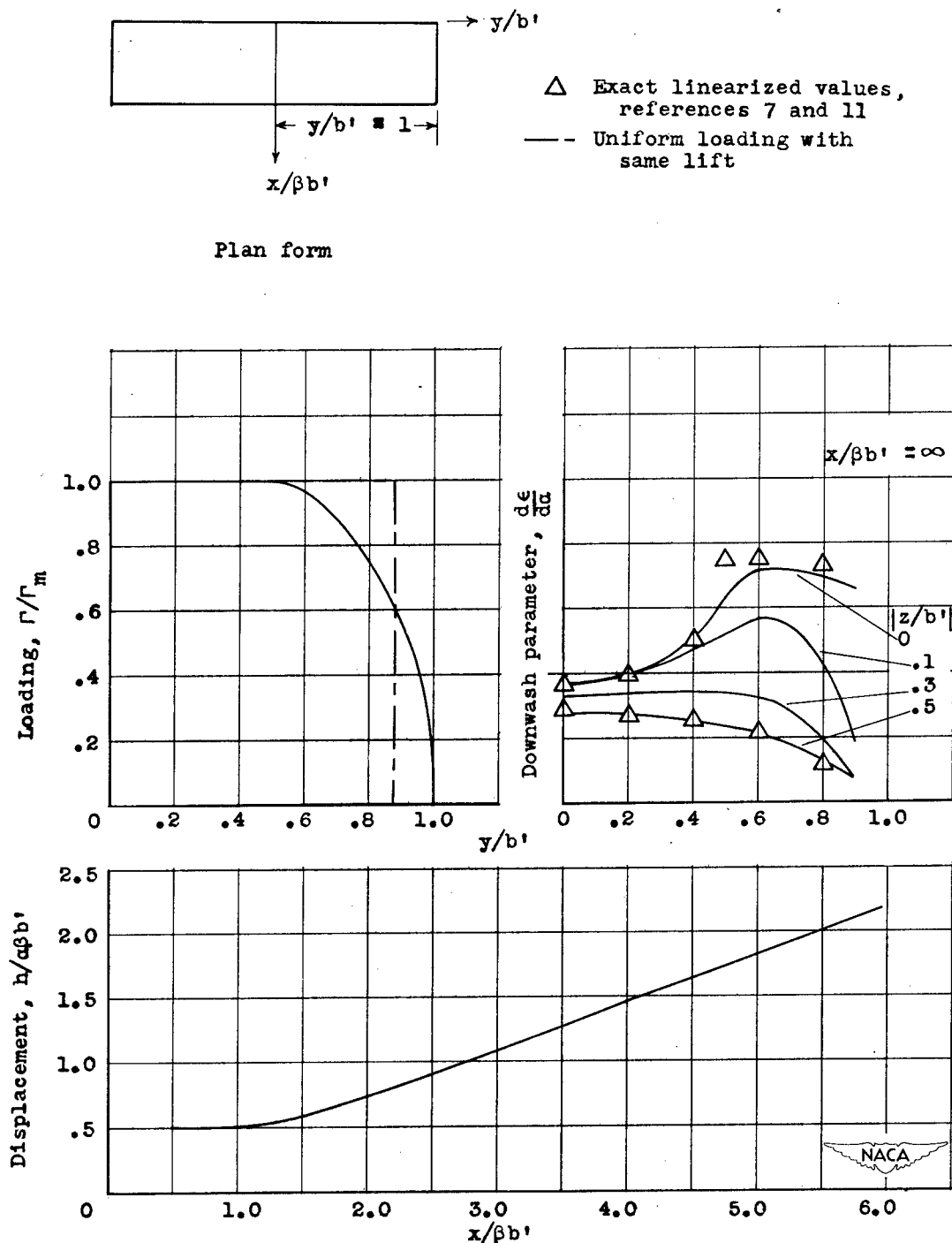
(a) Plan form, load distribution, downwash in Trefftz plane, and vortex-sheet displacement.

Figure 19. - Charts showing plan form, load distribution, downwash in Trefftz plane, vortex-sheet displacement, and downwash near wing. Reduced aspect ratio, 2; root chord, $1.000 \beta b'$; lift coefficient, $3.000 \alpha/\beta$; midspan circulation, $2.000 \alpha U b'$.



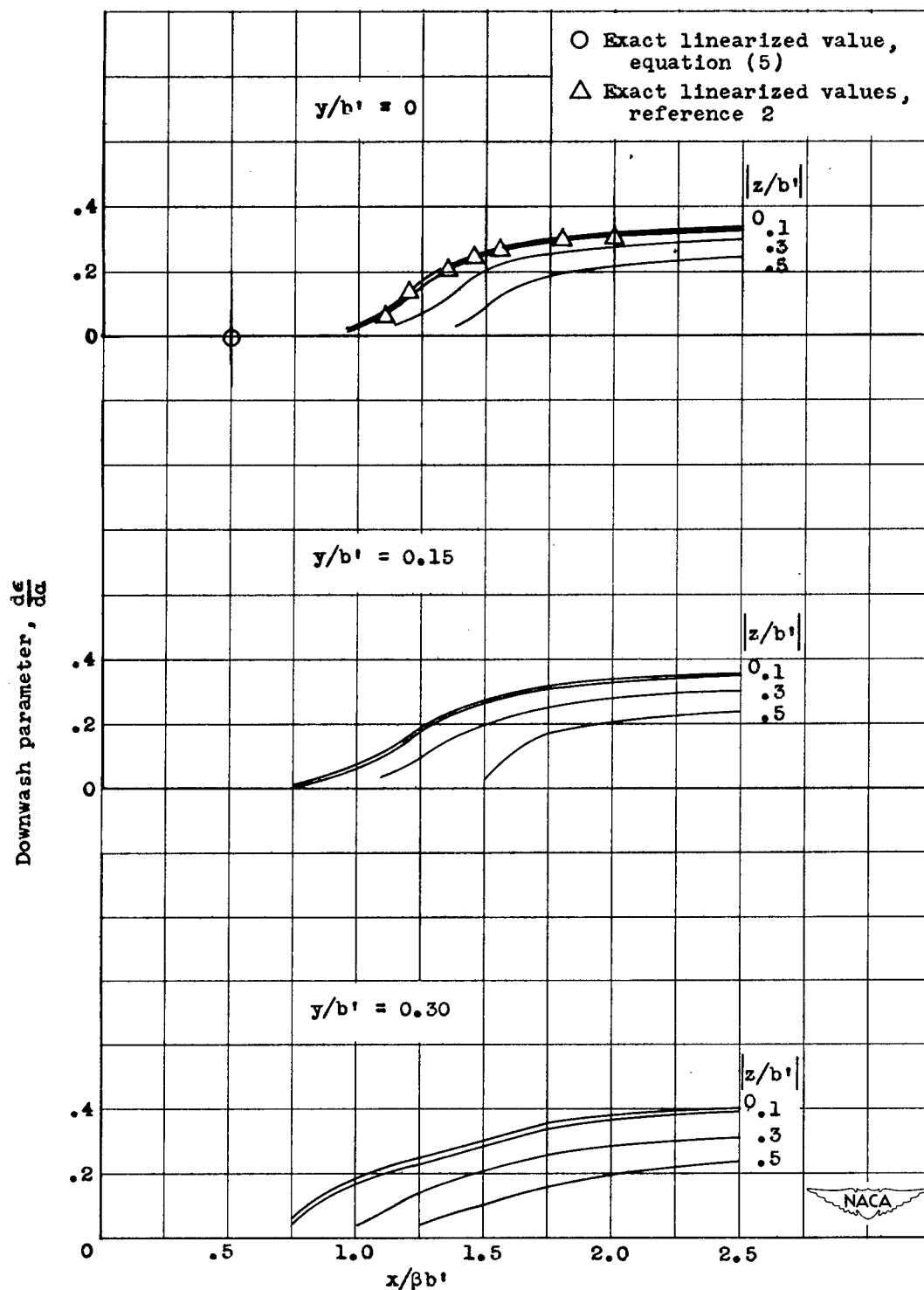
(b) Downwash near wing.

Figure 19. - Concluded. Charts showing plan form, load distribution, downwash in Trefftz plane, vortex-sheet displacement, and downwash near wing. Reduced aspect ratio, 2; root chord, $1.000 \beta b'$; lift coefficient, $3.000 \alpha/\beta$; midspan circulation, $2.000 \alpha U b'$.



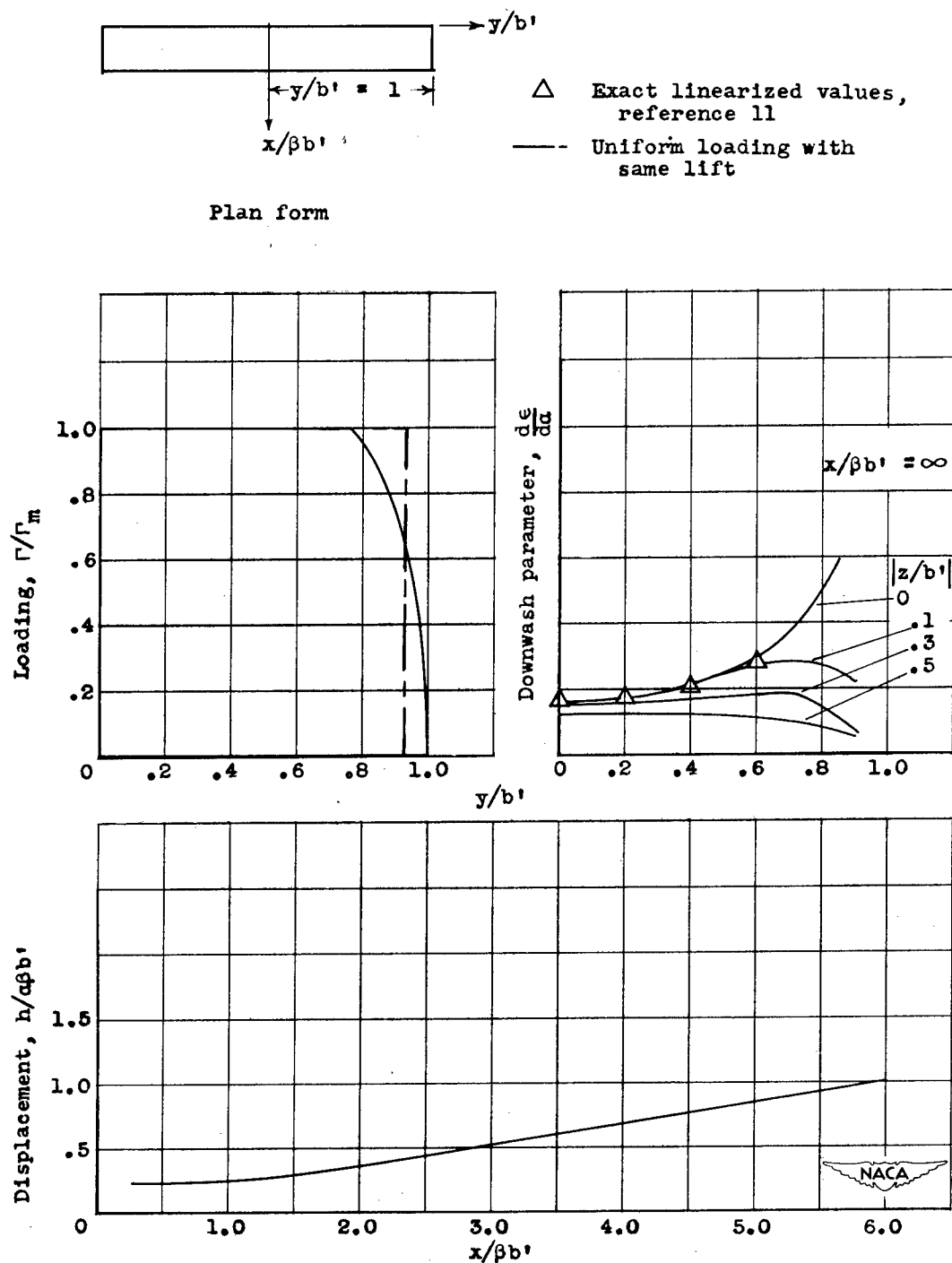
(a) Plan form, load distribution, downwash in Trefftz plane, and vortex-sheet displacement.

Figure 20. - Charts showing plan form, load distribution, downwash in Trefftz plane, vortex-sheet displacement, and downwash near wing. Reduced aspect ratio, 4; root chord, $0.500 \beta b'$; lift coefficient, $3.500 \alpha/\beta$; midspan circulation, $1.000 \alpha U b'$.



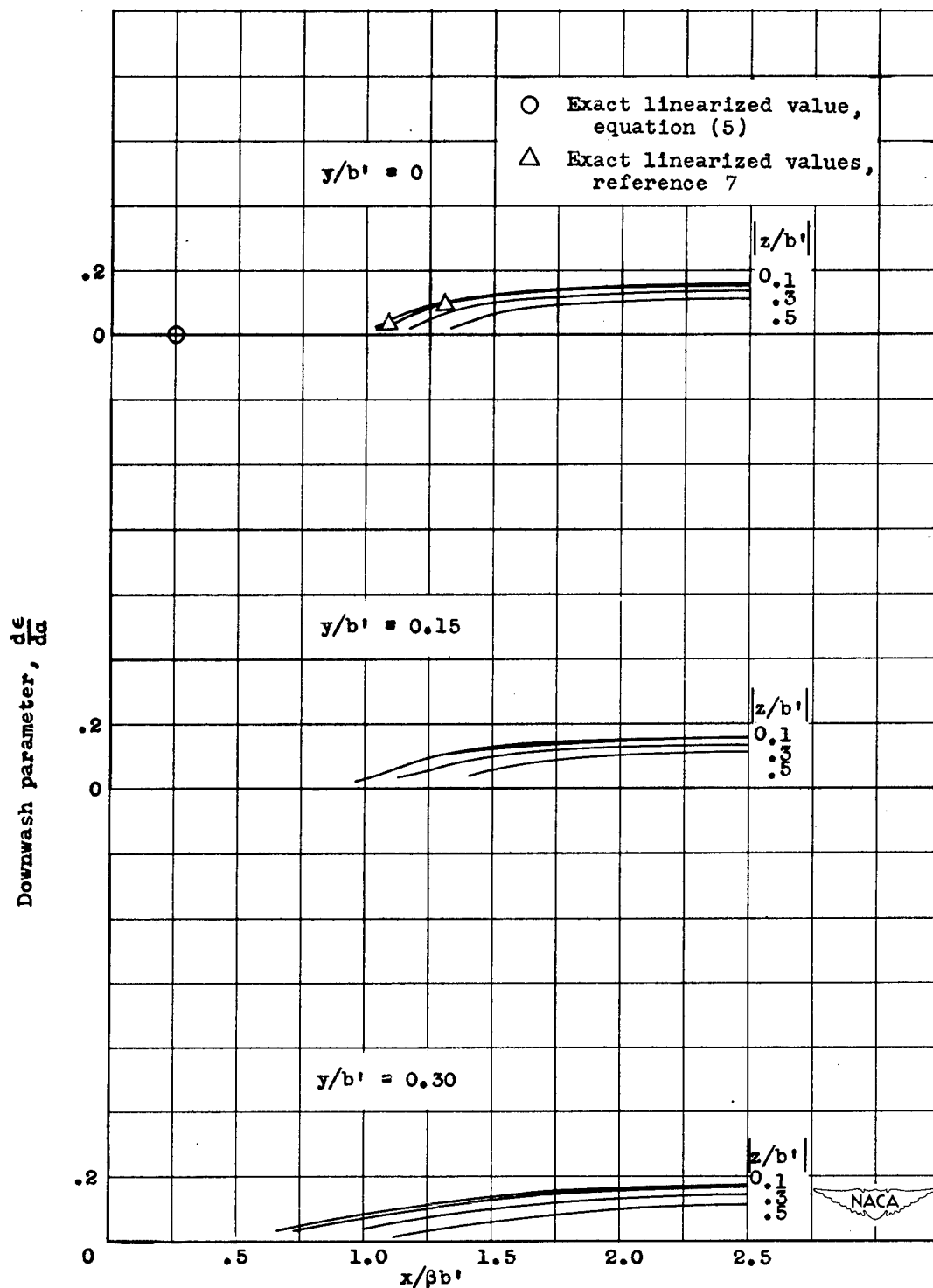
(b) Downwash near wing.

Figure 20. - Concluded. Charts showing plan form, load distribution, downwash in Trefftz plane, vortex-sheet displacement, and downwash near wing. Reduced aspect ratio, 4; root chord, $0.500 \beta b'$; lift coefficient, $3.500 \alpha/\beta$; midspan circulation, $1.000 \alpha U \beta b'$.



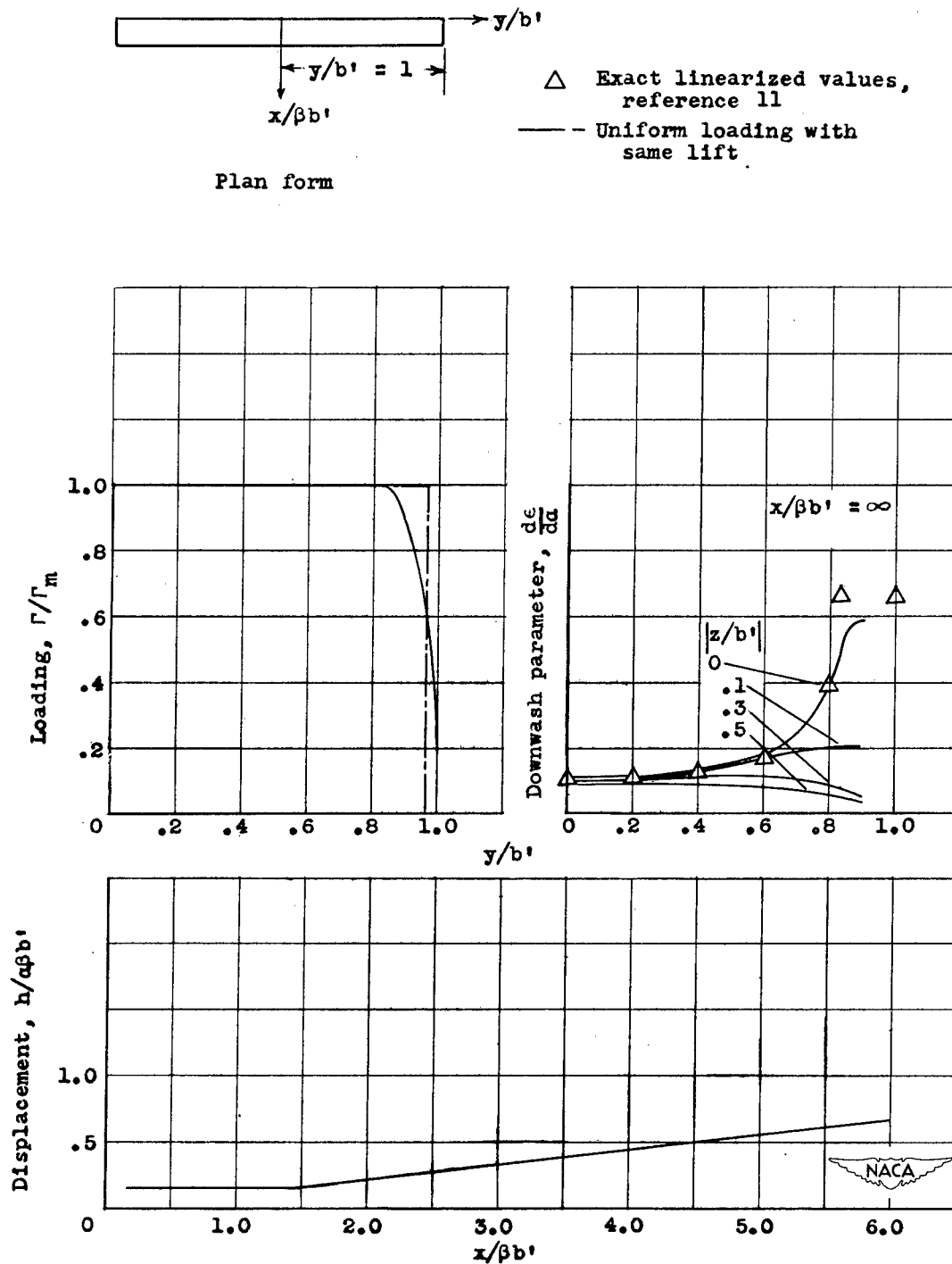
(a) Plan form, load distribution, downwash in Trefftz plane, and vortex-sheet displacement.

Figure 21. - Charts showing plan form, load distribution, downwash in Trefftz plane, vortex-sheet displacement, and downwash near wing. Reduced aspect ratio, 8; root chord, $0.250 \beta b'$; lift coefficient, $3.750 a/\beta$; midspan circulation, $0.500 aUb'$.



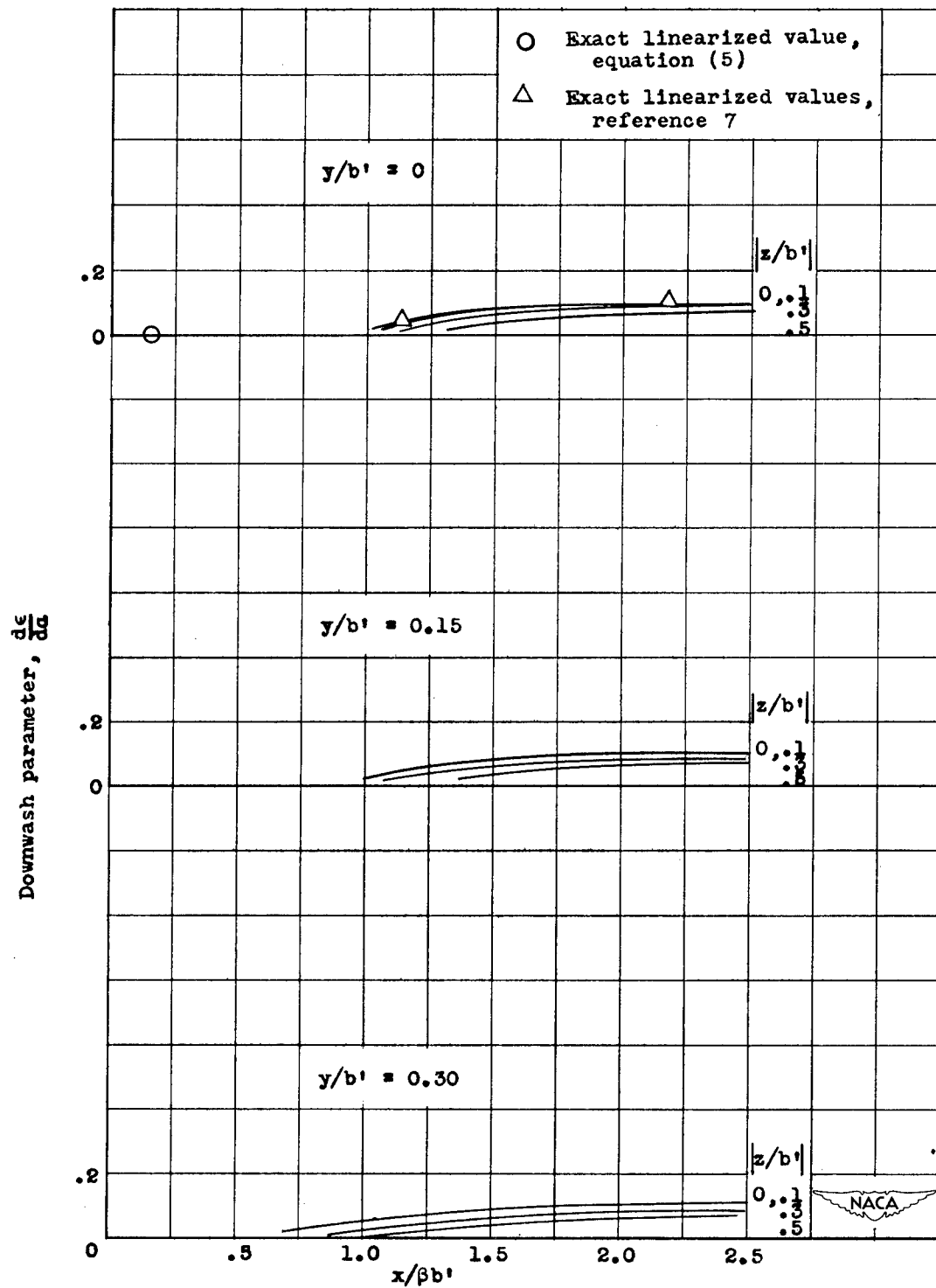
(b) Downwash near wing.

Figure 21. - Concluded. Charts showing plan form, load distribution, downwash in Trefftz plane, vortex-sheet displacement, and downwash near wing. Reduced aspect ratio, 8; root chord, $0.250 \beta b'$; lift coefficient, $3.750 \alpha/\beta$; midspan circulation, $0.500 \alpha U b'$.



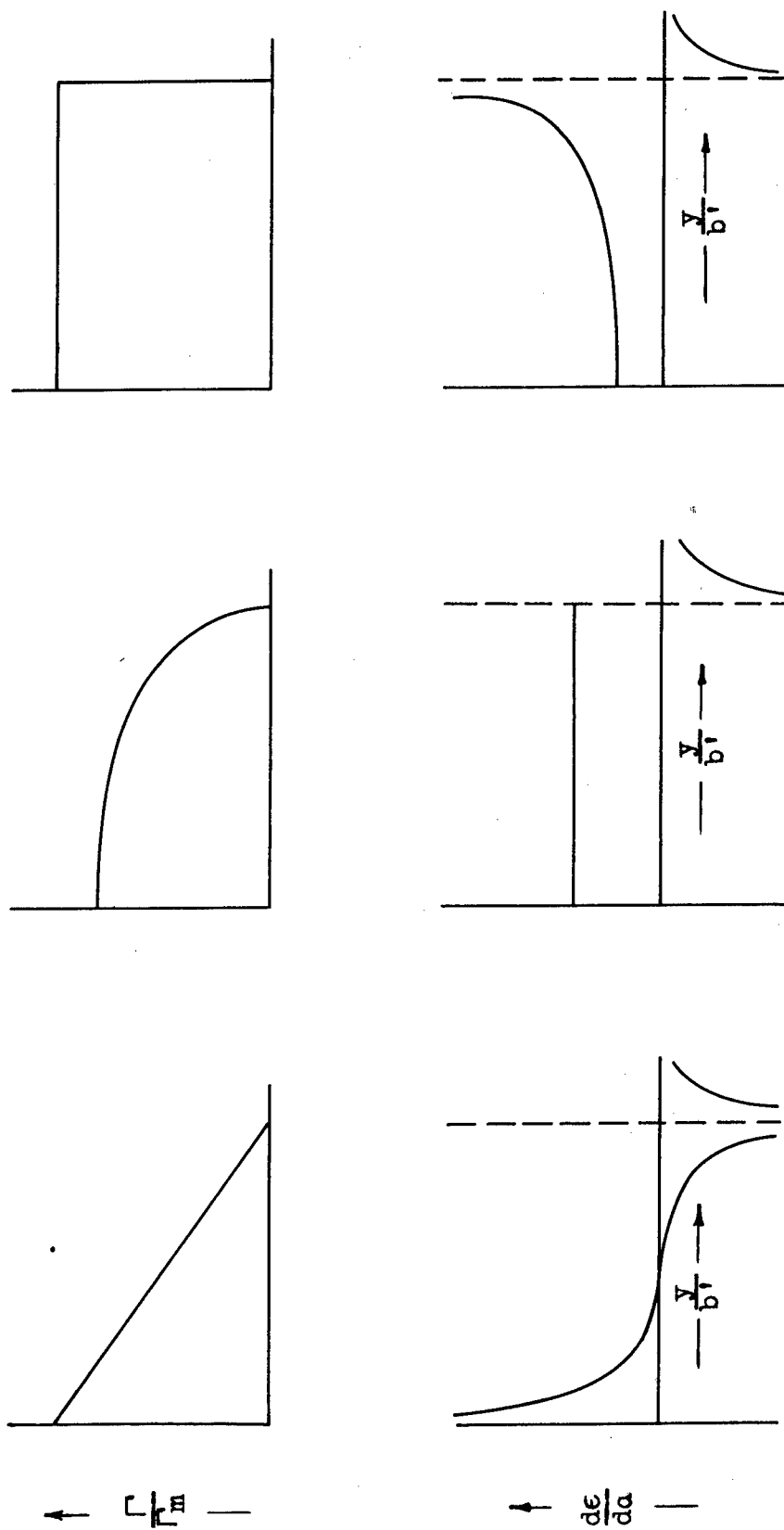
(a) Plan form, load distribution, downwash in Trefftz plane, and vortex-sheet displacement.

Figure 22. - Charts showing plan form, load distribution, downwash in Trefftz plane, vortex-sheet displacement, and downwash near wing. Reduced aspect ratio, 12; root chord, $0.167 \beta b'$; lift coefficient, $3.833 a/\beta$; midspan circulation, $0.333 aUb'$.



(b) Downwash near wing.

Figure 22. - Concluded. Charts showing plan form, load distribution, downwash in Trefftz plane, vortex-sheet displacement, and downwash near wing. Reduced aspect ratio, 12; root chord, $0.167 \beta b'$; lift coefficient, $3.833 \alpha/\beta$; midspan circulation, $0.333 \alpha U b'$.



(c) Uniform loading.

(b) Elliptical loading.

(a) Triangular loading.

Figure 23. - Spanwise load distributions and downwash in Trefftz plane ($z = 0$).

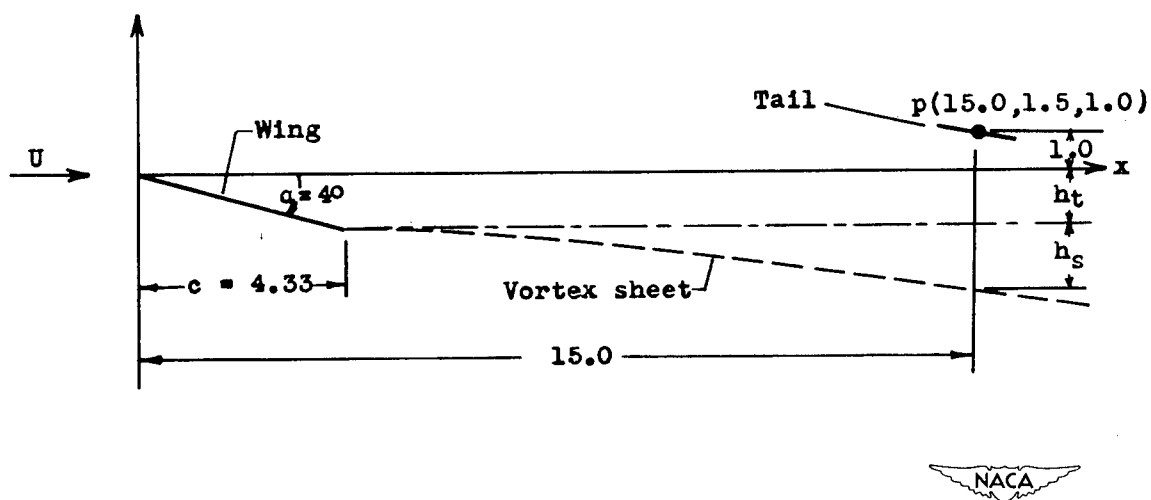


Figure 24. - Illustration for computed example (not to scale).